1 **Title:**

2 Morning and Evening Circadian Pacemakers Independently Drive Premotor Centers via a
3 Specific Dopamine Relay

4

5 **Authors:** Xitong Liang[1], Margaret C.W. Ho[2], Mark N. Wu[2], Timothy E. Holy[1] & Paul H.
6 Taghert[1]*

7

8 **Affiliations:**

9 1. Department of Neuroscience, Washington University in St. Louis, MO 63110, USA

10 2. Department of Neurology, Johns Hopkins University School of Medicine, Baltimore, MD
11 21205, USA

12 *Correspondence to: taghertp@pcg.wustl.edu

Abstract

Many animals exhibit morning and evening peaks of locomotor behavior. In *Drosophila*, previous studies identified two corresponding circadian neural oscillators: M (morning) cells which exhibit a morning neural activity peak, and E (evening) cells which exhibit a corresponding evening peak of activity. Yet we know little of how these distinct circadian oscillators produce specific outputs that regulate pre-motor circuits to precisely control behavioral episodes. Here we show that the Ring Neurons of the Ellipsoid Body (EB-RNs), a defined pre-motor center, display a spontaneous *in vivo* neural activity rhythm, with peaks in the morning and in the evening. The two EB-RN activity peaks coincide with the major bouts of locomotor activity and result from independent activation by M and E cells, respectively. Further, M and E cells regulate EB-RNs via two identified dopaminergic neurons PPM3-EB, which project to the EB and which are normally co-active with EB-RNs. Blocking the dopaminergic modulation onto EB-RNs prevents the daily two-peak pattern of neural activity in the EB-RN and greatly impairs circadian locomotor activity. These in vivo findings establish the fundamental elements of a circadian neuronal output pathway: distinct circadian oscillators independently drive a common pre-motor center through the agency of specific dopaminergic interneurons.

Main Text

Circadian rhythms provide adaptive value by promoting expression of diverse physiological processes and behaviors at specific times of the day. In mammals, rhythms in hormone release, rest/activity cycles, body temperature, and metabolism are all controlled by the multi-oscillator system of pacemakers in the suprachiasmatic nucleus (SCN) of the anterior hypothalamus. Numerous studies have documented that the SCN uses hormonal and neuronal signaling to provide adaptive phasic information across all times of day (Lehman *et al.,* 1987; Moore and Klein, 1974; Ralph *et al.,* 1990, De la Iglesia *et al.,* 2003; Kalsbeek *et al.,* 2006; VanderLeest *et al.*, 2007). However, the information connecting SCN signaling to neural circuits that translate its outputs is fragmentary. Lacking direct *in vivo* experimental observations, the definition of circadian output networks remains a significant challenge.

In *Drosophila*, a prominent circadian output is the daily locomotor activity rhythm, which peaks once around dawn and again around dusk (Figure 1c). The rhythm is controlled by molecular clocks that cycle synchronously within ~ 150 circadian pacemaker neurons (Nitabach & Taghert, 2008). Among these circadian neurons, two separate groups (termed M cells and E cells) control the morning and evening activity peaks respectively (Stoleru *et al.,* 2004; Grima *et al.,* 2004; Yoshii *et al.,* 2004). Previously we reported that different groups of circadian neurons display rhythmic but asynchronous circadian neural activity *in vivo*: they peak at different yet stereotyped times of day (Liang *et al.,* 2016). These neural activity rhythms depend on their synchronous molecular clocks, but their activity peak times are staggered, by neuropeptide-mediated interactions between circadian neuron groups. This allows the network to create multiple phasic time points (Liang *et al.,* 2017). Consequently, M cells peak in the morning and

E cells peak in the evening. The distinct peak times of M cells and E cells could potentially guide output motor circuits to generate independent morning and evening locomotor behavioral peaks.

Based on limited screens in *Drosophila*, two groups of identified peptidergic neurons were implicated in previous reports as components of output circuits for locomotor activity rhythms: specifically, these included neurons that express the diuretic hormone 44 (DH44), an orthologue of mammalian CRF (Cavanaugh *et al.,* 2014), and leucokinin (LK) (Cavey *et al.,* 2016), whose receptor is related to the neurokinin receptors. DH44 neurons receive synaptic inputs from DN1 pacemaker neurons, and both DH44- and LK- neurons are required for proper locomotor activity rhythms under constant darkness (DD) conditions (also see Yurgel *et al.,* 2018; Zawandala *et al.,* 2018). However, the connectivity by which these two groups of neuroendocrine neurons promote locomotor activity, and phase-restrict it to morning or evening times, is uncertain. The daily two-peak pattern of locomotor activity is different from the daily activity pattern of either LK neurons (which are more active in the evening - Cavey *et al.,* 2016), or that of DH44 neurons (which are more active in mid-day - Bai *et al.,* 2018). These observations suggest that robust circadian locomotor timing information is likely to utilize additional pre-motor regulatory centers. As a strategy, we reasoned that spontaneous activity patterns corresponding to the daily bimodal activity pattern could help identify critical pre-motor elements.

Robie *et al.* (2017) performed an unbiased screening of sparsely-labeled neuronal groups to determine which could initiate locomotor activity. By this analysis, the strongest candidates were the Ring Neurons of the Ellipsoid Body (EB-RNs) (Figure 1a). In parallel, silencing these same EB-RNs reduced spontaneous locomotor activity (Martín-Peña *et al.,* 2014). EB-RNs are a subset of neurons that constitute the Central Complex - the primary locomotor control center in

insects (Strauss and Heisenberg, 1993; Pfeiffer and Homberg, 2014). EB-RNs encode visual landmarks for visuospatial-memory-based orientation and navigation (Neuser *et al.,* 2008; Ofstad *et al.,* 2011; Seelig and Jayaraman, 2013). In the monarch butterfly, EB-RNs are involved in sun-compass navigation (Heinze and Reppert, 2010), which requires timing information from circadian clocks (Froy *et al.,* 2003). In *Drosophila,* EB-RNs might also be regulated by the neuropeptides LK (Cavey *et al.,* 2016) and the pigment-dispersing factor (PDF) (Pírez *et al.,* 2013). Therefore, we first measured spontaneous activity in EB-RNs *in vivo*, to see if they represent a point of convergent circadian regulation that could lead to daily bouts of locomotor activity.

Spontaneous daily bimodal activity in EB-RNs *in vivo*

To test whether EB-RNs regulate circadian locomotor activity, we expressed tetanus toxin light chain (TeTn, Sweeney *et al.,* 1995) to block neurotransmission in the majority of ~60 EB-RNs. As expected, the circadian rhythm of locomotor activity in these flies was impaired under DD, as was the general level of activity (Figure 1b and Extended Data Table 1). Therefore, to learn about the possible involvement of the EB-RNs in normal rhythmic locomotion (Figure 1c), we then measured *in vivo* spontaneous activity exhibited by these neurons in otherwise wild-type flies. Using the genetically encoded calcium sensor GCaMP6s (Chen *et al.,* 2013), we performed *in vivo* Ca^{2+} imaging in living flies for 24 hrs using methods previously described (Liang *et al.,* 2016, 2017). EB-RNs contains several genetically and morphologically distinct subgroups (Renn *et al.,* 1999a). We dissected four EB-RN subgroups using different genetic drivers that use regulatory sequences associated with different circadian clock-related genes: one with sequences from *timeless,* one from *cryptochrome,* and two from *pdfr (pigment-dispersing factor receptor)* (Figure 1d-g and Extended Data Figure 1a). In both 12-hr light: 12-hr dark (LD)

cycles and in constant darkness (DD) conditions, the four different EB-RN subgroups we tested displayed spontaneous, daily Ca^{2+} rhythms (Figure 1e-g). The average Ca^{2+} activity profile of each subgroup was bimodal (Hartigans' dip test, LD: $p<0.0001$, DD: $p<0.05$), with a peak around dawn and another around dusk. These peaks corresponded to the times of day when flies showed daily locomotor activity peaks (Figure 1c). The outer subgroup of EB-RNs caused the strongest effects on locomotor activity according to Robie *et al.* (2017). We tested the same split-GAL4 drivers as reported by Robie *et al.* (2017) and found that these locomotion-promoting EB-RNs likewise displayed a similar spontaneous daily bimodal activity pattern (Extended Data Figure 1b; Hartigans' dip test, $p<0.0001$). We also confirmed the daily bimodal activity pattern exhibited by different EB-RN subgroups using a separate, circadian-clock-irrelevant driver line to label the majority of EB-RNs (Figure 1h; Hartigans' dip test, LD: $p<0.001$, DD: $p<0.01$).

To directly test the correlation between EB-RN neural activity and locomotor activity in single flies in our experimental paradigm, we performed *in vivo* 24-hr Ca^{2+} imaging while simultaneously measuring spontaneous leg movements as a proxy for locomotor activity levels (Figure 2a). EB-RN activity was strongly correlated with such behavioral activity in individual flies, both at a daily time scale (Figure 2f-h) as well as at a shorter (hourly) time scale (Figure 2c-e). Analysis of the shorter timescale indicated that increases in EB-RN activity were coincident with increases in behavioral activity; decreases typically preceded decreases in behavioral activity by a few minutes (Figure 2E). Thus, EB-RNs, consistent with their documented roles as pre-motor activity centers, exhibit spontaneous daily neural activity rhythms that precisely correspond to the pattern of circadian locomotor rhythms.

Circadian pacemaker neurons drive EB-RN activity rhythms

The daily neural activity rhythms in EB-RNs could reflect rhythmic sensory inputs, either proprioceptive or visual. For example, recent studies suggest that EB-RNs encode self-motion information (Shiozaki & Kazama, 2017). Therefore, to block ascending proprioceptive sensory inputs, we transected connectives between the brain and ventral nerve cord (between subesophageal and first thoracic neuromeres) immediately before Ca^{2+} imaging. EB-RNs still displayed normal bimodal activity rhythms (Figure 3a). These EB-RN rhythms persisted even when the entire body of the fly was removed immediately before imaging (Figure 3b). Therefore, spontaneous bimodal EB-RN activity rhythms are not a consequence of locomotor behavioral activity. Previous studies also showed that EB-RNs receive large-scale visual inputs (Seeling & Jayaraman, 2013; Omoto *et al.,* 2017; Sun *et al.,* 2017). We therefore removed visual inputs by testing flies in DD (Figure 1) or by testing genetically blind $norpA^{P24}$ mutant flies (Figure 3c): in both cases, normal EB-RN activity rhythms persisted. Together, these results demonstrate that EB-RN activity rhythms are not driven by daily rhythmic sensory inputs.

To determine if EB-RN activity rhythms are driven by molecular clocks, we measured Ca^{2+} activity in circadian-defective per^{01} (null) mutant flies (Konopka & Benzer, 1971), which fail to display circadian clock-dependent anticipatory behavior. Although per^{01} flies still had two peaks of startle responses (to the lights-on and lights-off stimuli under LD cycles), daily Ca^{2+} activity patterns in EB-RNs were arrhythmic (Figure 3d). Therefore, EB-RN activity rhythms specifically correlate with - and entirely depend on - circadian clock signals that regulate daily behavioral peaks. Notably, EB-RNs exhibit no measurable expression of the core clock gene *period*, which is highly expressed and cycling in circadian pacemaker neurons (Extended Data Figure 1c) (Kaneko and Hall, 2000). Furthermore, manipulations to alter the pace of circadian clocks in a subset of circadian neurons shifted the locomotor activity phases as previously

reported (Stoleru *et al.,* 2005; Yao and Shafer, 2014), while the same manipulation within EB-RNs did not affect locomotor behavior (Extended Data Figure 1d-f). Thus, we conclude that daily EB-RN activity rhythms are downstream of circadian timing information provided by circadian pacemaker neurons. To test whether circadian neurons regulate EB-RNs, we impaired a crucial signal within the pacemaker network, the neuropeptide PDF (Renn *et al.,* 1999b). In PDF receptor mutant (*pdfr*^{han5304}) flies, the EB-RNs activity pattern under LD transformed to a daily unimodal one (Hartigans' dip test, p=0.23): the morning activity peak was lost, and the evening peak was advanced (Figure 3e; Watson-Williams test, p=0.00012). This neural activity pattern mirrors the changes in locomotor activity pattern typically displayed by *pdfr*^{han5304} flies (Han *et al.,* 2005). Meanwhile, EB-RNs responded to thermogenetic and pharmacogenetic activation of PDF-releasing neurons (Extended Data Figure 2ab). Thus, EB-RN activity rhythms could be driven (directly or indirectly) by PDF-expressing circadian pacemaker neurons.

Circadian neurons dictate phases of EB-RN activity

In contrast to EB-RNs, all circadian pacemaker neurons showed single daily peaks of activity. This difference suggested that the daily two-peak activity pattern of EB-RNs could be generated by a combination of different circadian neuronal outputs. For example, M cells could drive a morning activity peak in EB-RNs while E cells could independently drive EB-RN evening activity. We found that EB-RNs responded to the selective activation of M cells (four s-LNv) by ATP application to brains expressing ATP-gated cation channel P2X2 (Lima and Miesenböck, 2005) in M cells (Figure 4a). A similar design to selectively activate E cells, the 5th s-LNv and three PDFR-positive LNd (Im and Taghert, 2011), produced correspondent EB-RN responses of comparable amplitude (Figure 4b and Extended Data Figure 2de). These results support the proposition that both M cells and E cells have functional connections with EB-RNs.

As a more stringent test, we then asked whether selectively accelerating M or E oscillators would selectively influence the phase of either the morning and/or evening peak of EB-RN Ca^{2+} activity. Overexpressing Shaggy (SSG) using *pdf-GAL4* (PDF>SGG) to accelerate the molecular clocks selectively in Morning oscillators advanced the morning peak of locomotor activity (cf. Stoleru *et al.,* 2005) and the M-cell activity peak (Figure 4de). In these flies, we found that only the morning peak of EB-RN Ca^{2+} activity was phase-advanced, while their evening Ca^{2+} peak phase was unaffected (Figure 4f-h). This result suggests that the morning peak of EB-RNs activity is dictated by the morning peak of M cell activity. We then in parallel asked whether the evening peak of EB-RNs is dictated by the evening peak of E cells. Overexpressing SGG in E cells by *dvpdf-GAL4* and *pdf-GAL80* (E-cell>SGG) advanced both morning and evening behavioral peaks in 12 hr light: 12 hr dark cycles (Extended Data Figure 3), yet it selectively advanced the evening behavioral peak in a short-day condition (10 hr light: 14 hr dark cycles; cf. Stoleru *et al.,* 2007). Whether this results from the different photoentrainment conditions, or from faulty suppression of M cell activity by the GAL80 element awaits further study. In short day, when the E-cell peak was selectively phase-advanced (Figure 4i-l), the evening peak of EB-RN Ca^{2+} activity was selectively phase-advanced, and by comparable amplitude (Figure 4k-m). Taken together, these results reveal essential circuit links to demonstrate that M cells and E cells can independently dictate the two phases of EB-RN pre-motor activity.

Dopaminergic neurons regulate EB-RNs

None of the ~150 circadian pacemaker neurons in *Drosophila* project directly to the EB (Helfrich-Förster, 2005). We therefore asked through which interneurons M cells and E cells might regulate daily neural activity in EB-RNs. A set of two dopaminergic (DA) neurons (named

189 PPM3-EB) appeared as prominent candidates: they innervate the EB; further, they can initiate
190 locomotor activity and promote ethanol-induced locomotor activity (Kong *et al.,* 2010). First we
191 established that PPM3-EB neurons spontaneously displayed a daily bimodal neural activity
192 pattern *in vivo* (Hartigans' dip test, $p<0.0001$), similar to that of the EB-RNs and similar to the
193 profile of locomotor activity (Figure 5a). To study the precise relationship between activity in
194 EB-RNs and that in PPM3-EBs in single fly brains, we employed dual-color Ca^{2+} imaging. This
195 method separated Ca^{2+} activity signals from these two anatomically-overlapping neuron groups,
196 by simultaneously recording a green signal (GCaMP6s) in PPM3-EB and a red signal (jGECO1a,
197 Dana *et al.,* 2016) in EB-RNs (Figure 5b). We found that the spontaneous Ca^{2+} activity patterns
198 of EB-RNs were highly correlated with those of PPM3-EB, but poorly correlated with those of
199 the l-LNv circadian neurons, which were also labelled by jGECO1a (Figure 5c-f). This result
200 suggests that PPM3-EB and EB-RNs are closely connected: they receive common inputs and/or
201 one receive synapses from the other.
202 Furthermore, both PPM3-EB and EB-RNs responded to the bath-application of PDF and
203 the pharmacogenetic activation of PDF neurons (Extended Data Figure 4ab). In response to the
204 activation of PDF neurons, PPM3-EB responded more quickly than did EB-RNs, which is
205 consistent with placing PPM3-EBs 'upstream' of EB-RNs. Indeed, EB-RNs also responded to
206 the bath-application of dopamine (Extended Data Figure 4c) and to the activation of PPM3-EB
207 (Extended Data Figure 4d). Together these results support a model in which circadian pacemaker
208 neurons indirectly activate as many as ~60 pairs of EB-RNs by first activating two pairs of
209 dopaminergic neurons, the PPM3-EB. We tested this model by blocking neurotransmission in
210 PPM3-EB neurons, thereby asking if their specific output is necessary for proper locomotor
211 rhythmicity. Using intersectional genetics (*GMR92G05-GAL4* and *TH-Flp*), we restricted the

212 expression of tetanus toxin (TeTn, Sweeney *et al.,* 1995) to the two pairs of PPM3-EB. The
213 locomotor activity of these flies was largely arrhythmic under DD (Figure 5gh). This behavioral
214 deficit was comparable with, and even more severe than that caused by blocking
215 neurotransmission in the majority of EB-RNs (Figure 1b and Extended Data Table 1).
216 Importantly, while the molecular clocks and Ca^{2+} rhythms of circadian pacemaker neurons in
217 these flies were intact, the daily bimodal neural activity pattern of EB-RNs was severely
218 impaired (Extended Data Figure 5 and Figure 5ij). Likewise, knocking down DA receptors
219 DopR2 or D2R in the majority of EB-RNs also impaired rhythmicity in locomotor activity under
220 DD (Figure 5k and Extended Data Table 1). Hence we propose that dopaminergic input from
221 PPM3-EB neurons forms a critical relay to instruct EB-generated locomotor activity according to
222 a multi-phasic circadian schedule.

223 **Discussion**

224 Locomotor activity in *Drosophila* follows a daily bimodal rhythm that peaks around
225 dawn and again around dusk. By measuring spontaneous neural activity *in vivo* across the 24 hr
226 day, we found that morning and evening circadian oscillators independently activate the pre-
227 motor Ring Neurons of the Ellipsoid Body through the agency of PPM3-EB dopaminergic
228 neurons. These findings provide the most detailed insights available in any model system by
229 which pre-motor pathways are organized in response to phasic circadian pacemaker information.
230 In addition, they indicate an unexpectedly obligate role for dopamine in the neural control of
231 daily rhythmic locomotor activity. We based our conclusions on four lines of evidence: (1) Both
232 PPM3-EB and EB-RNs display daily spontaneous bimodal neural activity patterns that precisely
233 correlate with locomotor activity patterns peaking around dawn and dusk (Figure 1 & 5a). (2)
234 Locomotor activity closely followed changes in EB-RN activity (Figure 2) while EB-RN activity

was itself highly correlated with PPM3-EB activity (Figure 5b-f). (3) Different phases of EB-RN circadian-rhythmic neural activity relied on independent inputs from circadian pacemakers, M cells and E cells, but did not rely at all on visual inputs or on the execution of locomotor behavior (Figure 3 and 4). (4) Both EB-RN activity rhythms and normal locomotor activity rhythms required PPM3-EB inputs (Figure 5g-j); normal locomotor activity rhythms also required DA receptors on EB-RNs to receive inputs from PPM3-EB DA neurons (Figure 5k). These data together support a model that features outputs from M cells and E cells sequentially and independently generating the two daily peaks of activity PPM3-EB DA neurons. These non-circadian PPM3-EB DA neurons in turn relay the phasic information to activate as many as ~60 pairs of EB-RNs, thereby generating the bimodal daily locomotor activity rhythm (Figure 5l).

Our findings constitute important steps in relating the activities of distinct circadian pacemaker neurons to downstream neural circuits. Selcho et al. (2017) recently described circadian pacemaker control of a peripheral clock in *Drosophila* to control steroid hormone secretion and, whose titres gate subsequent adult emergence (eclosion). In that output pathway, s-LNv activate the peptidergic PTTH neurons, which in turn activate the peripheral Prothoracic Gland. With respect to locomotor behavior, we found that M (s-LNv) cells and E (LNd) oscillators independently control the morning and evening neural activity phases in EB-RNs (Figure 4). Two recent studies linked a different subset of circadian pacemakers (DN1s) to subgroups of EB-RNs, via subsets of neurons in the Anterior Optic Tubercle (Lamaze *et al.,* 2018; Guo *et al.,* 2018). By manipulating activity in this pathway, both groups found effects on the balance between sleep and wake states. Thus, increasing lines of research indicate circadian- and sleep-regulating circuits impart timing information to govern behavior through the classic pre-motor centers of the Central Complex.

Previous studies in flies and mice have shown that DA modulates circadian pacemaker circuits (Chang *et al.,* 2006; Grippo *et al.,* 2017; Hirsh *et al.,* 2010; Klose *et al.,* 2016; Langraf *et al.,* 2016; Shang *et al.,* 2011, 2013). Our findings here show that circadian pacemaker neurons also regulate DA neuron activity. DA neurons responded to circadian neuron outputs (Extended Data Figure 4ab) and showed spontaneous circadian neural activity rhythms that were correlated with behavior (Figure 5a). These findings correspond to earlier studies in mammals showing that circadian rhythms in DA neuron activity, and in striatal DA content, are dependent on master circadian pacemaker neurons in the suprachiasmatic nuclei (SCN) (Smith *et al.,* 1992; Sleipness *et al.,* 2006; Luo *et al.,* 2008; Fifel *et al.,* 2018). Deficits of DA neurons in patients and in animal models of Parkinson's disease caused dysregulation of circadian locomotor activity patterns and of sleep (Videnovic and Golombek, 2017). Consistent with our model, a DA-deficient mouse model displays dampened and fragmented locomotor activity rhythms, yet possesses normal SCN molecular clocks (Taylor *et al.,* 2009; Kudo *et al.,* 2011). It remains to be determined whether DA in mammals, as in *Drosophila*, represents the critical agent by which circadian outputs activate pre-motor centers to adaptively schedule locomotor activity.

The effects of DA to organize proper circadian control of locomotor behavior may be related to its well documented effects in *Drosophila* to promote arousal, especially forms of arousal associated with changes in sleep and circadian rhythm states (Andretic *et al.,* 2005; Birman, 2005; Kume *et al.,* 2005; Lima and Miesenbock, 2005; Lebestky *et al.,* 2009; Liu *et al.,* 2012). A recent study suggests that PDF signals from circadian neurons promotes wakefulness by suppressing daytime activity in the PPM3 DA neurons (Potdar and Sheeba 2018). However, we favor an alternative model which is based on the results described above, including both manipulations of PPM3 physiology as well as measurements of normal PPM3 24-hr activity

281 patterns *in vivo*. We propose PPM3-DA neurons promote wakefulness and locomotor activity in
282 the morning by excitation from the M oscillators, and perhaps directly by PDF.

283 Our results suggest that a major influence of circadian timing signal on locomotor
284 activity is in the Central Complex (CX), the decision-making circuit that dictates the balance
285 between locomotion and rest. Within the CX, EB neurons transform sensory inputs into goal-
286 directed motor outputs (Sun *et al.,* 2017; Shiozaki and Kazama, 2017). The final motor output is
287 subject to many signals reflecting the internal state: for example, hunger signals transmitted
288 through the leucokinin-expressing neurons promote locomotor activity (Yurgel *et al.,* 2018;
289 Zandawala *et al.,* 2018). Here, we propose that the circadian system promotes locomotor activity
290 in the dawn and dusk episodes by increasing the probability of the EB-RNs to favor activity over
291 rest. A similar action on EB-RNs appears to underlie sleep promotion by dorsal fan-shaped body
292 (dFSB) neurons (Donlea *et al.*, 2017). dFSB neurons effectively suppress sensory-triggered
293 movements by inhibiting EB-RNs via helicon cells and thereby instigate less activity and more
294 rest. Thus, sleep and circadian signaling antagonistically converge on the EB-RN system to
295 influence the level of motor output.

296 In addition to motor outputs, parts of EB circuit also signal the sleep drive: Liu *et al.*
297 (2016) showed that a subgroup of EB-RNs, R2 (called R5 by Omoto *et al.,* 2017) registers sleep
298 debt and thereby constitutes an integral part of the sleep homeostat mechanism. How can this be
299 reconciled with our finding that the EB-RNs (including R2s) exhibit neural activity in concert
300 with locomotor behavior? We propose that, because the level of locomotor activity is directly
301 encoded by EB-RN activity, a subgroup of them (R2s) incorporates the amount of locomotor
302 activity along with duration of wakefulness to help generate sleep drive. Therefore, although
303 they receive common circadian pacemaker and DA inputs, and although they exhibit common

304 activation periods at dawn and at dusk, different subgroups of EB-RNs likely have specialized

305 downstream functions in behavioral control.

306 **Figure legends**

307 **Figure 1. Daily bimodal neural activity patterns of EB ring neurons.** (**a**) The ellipsoid body
308 ring neurons (EB-RNs) in the fly brain. (**b**) Average rhythm strength (power) of locomotor
309 activity for 9 days under constant darkness (DD) of control and flies with TeTn expressed in EB-
310 RNs; asterisk denotes significant differences compared to control ($P < 0.0001$, Mann-Whitney
311 test). (**c**) The average locomotor activity histogram and phase distributions of behavioral peaks of
312 wild type *R56H10-GAL4/GCaMP6s* flies (left) under 12-hr light: 12-hr dark (LD) cycle and
313 (right) in the first day under DD (n = 16 flies). Dots indicate SEM. (**d-h**) Daily Ca^{2+} activity
314 patterns of the EB ring neuron subgroups: (d) R1 labelled by *tim-GAL4*, (e) R2 labelled by *cry-*
315 *lexA*, (f) R3 labelled by *pdfr(F)-GAL4*, (g) R4 labelled by *R19H08(pdfr)-lexA*, and (h) R1-4
316 labelled by *R56H10-GAL4*. Left, confocal images of EB ring neurons and diagrams of their
317 concentric arborization radii; scale bars, 25 μm. Middle and Right, average Ca^{2+} transients and
318 Ca^{2+} phase distribution for both morning peaks (orange dots and arrow) and evening peaks (blue
319 dots and arrow). Middle - under LD; Right - under DD.
320
321 **Figure 2. EB ring neuron activity is correlated with locomotor activity.** (**a**) Illustration of
322 long-term *in vivo* imaging with infrared measurement of locomotor activity (see Methods). (**b**)
323 Map of the major circadian neuron groups and EB ring neurons. (**c**) Representative recordings of
324 two flies: bars, normalized locomotor activity counts per 10 m; blue traces, Ca^{2+} activity of EB-
325 R2 neurons in the same fly. (**d-e**) Average locomotor activity (black) and Ca^{2+} activity (blue)
326 aligned by (d) increasing phase and (e) decreasing phase of Ca^{2+} activity. The averaged phase
327 lags were calculated by cross-correlation: (c) 0.35 ±7 min; (d) -15±0.5 min. (**f-h**) Average

328 locomotor activity (f) and average Ca^{2+} transients of (g) EB-R2 neurons and (h) circadian
329 pacemaker neurons in the same flies (n = 6 flies). Dots and shading indicate SEM.
330
331 **Figure 3. EB ring neuron rhythms are driven by clocks, not in response to behavior or**
332 **sensation.** (**a**) Daily Ca^{2+} activity patterns of (middle) EB-R2 neurons and (right) circadian
333 neurons under LD immediately after cutting the connectives between brain and ventral nerve
334 cord (n = 10 flies). (**b**) Daily Ca^{2+} activity patterns of EB-R2 and circadian neurons under LD
335 immediately after removing the bodies (n = 6 flies). (**c**) In blind *norpA*^{p24} mutant flies, (left)
336 average locomotor activity (n = 22 flies) and daily Ca^{2+} activity patterns (middle) of EB-R2
337 neurons and (right) circadian neurons under LD (n = 6 flies). (**d**) In *per*^{01} mutants, average
338 locomotor activity (n = 16 flies) and arrhythmic Ca^{2+} activity patterns of EB-R2 and of circadian
339 neurons under LD (n = 7 flies). (**e**) In *pdfr*^{han5304} mutants, average locomotor activity (n = 8 flies)
340 and Ca^{2+} activity patterns of EB-R2 and of circadian neurons under LD (n = 7 flies).
341
342 **Figure 4. Daily activity phases of EB-RNs are dictated by M and E cells.** (**a**) Illustration and
343 averaged response traces of M cells (s-LNv) and EB-R2 neurons to ATP application in flies with
344 P2X2 expressed in M cells (n = 6 flies). (**b**) Illustration and averaged response traces of E cells
345 (three LNd and the 5th s-LNv neurons) and EB-R2 neurons to ATP application in flies with P2X2
346 expressed in E cells (n = 5 flies). (**c**) Maximum Ca^{2+} changes of EB-R2 after ATP application in
347 (a), (b), and control (n = 3 flies). (**d**) Average locomotor activity in DD1 of (top) wild type (WT,
348 n = 16 flies) and (bottom) flies expressing SGG in PDF neurons (PDF>SGG, n = 24 flies). (**e**)
349 Phases comparisons of morning and evening activity between WT and PDF>SGG. Note that
350 only the morning activity phase was advanced (* $P < 0.05$, Watson-Williams test). (**f-g**) Daily

Ca^{2+} activity patterns of (left) circadian neurons and (right) EB-R2 neurons (c) in WT flies under DD (n = 12 flies) and (d) neurons in PDF>SGG flies under DD (n = 6 flies). (**h**) Phase comparison of each circadian neuron group and for both morning peaks (orange) and evening peaks (blue) of EB-R2 neurons between WT and PDF>SGG flies. Note that only M cells (s-LNv) and the morning peak of EB-R2 were significantly advanced in PDF>SGG. (**i**) Average locomotor activity of (top) WT (n = 13 flies) and (bottom) flies expressing SGG in E cells (E-cells>SGG, n = 16 flies) in DD1 after 5 cycles of 10 h light: 14 h dark (short day, SD). **(j)** Phase comparisons of morning and evening activity between WT and E-cell>SGG. Note that only evening activity phases were significantly advanced. (**k-l**) Daily Ca^{2+} activity patterns and phase comparisons of (left) circadian neurons (PDF neurons were invisible due to *pdf-GAL80*) and (right) EB-R2 neurons in (k) WT and (l) E-cells>SGG flies after SD entrainment (n = 5 flies). s-LNv and l-LNv were invisible due to *pdf-*. (**m**) E cells (LNd) and the evening peak of EB-R2 were significantly advanced in E-cells>SGG flies compared to WT ones.

Figure 5. PPM3-EB and EB-RNs constitute a circadian output motor circuit. (**a**) Daily bimodal Ca^{2+} activity patterns of PPM3-EB under LD and DD (n = 6 and 6 flies). (**b**) Illustration of dual-color Ca^{2+} imaging: GCaMP6s in PPM3-EB and jRGECO1a in EB-R2 and circadian neurons. (**c**) Example traces of Ca^{2+} activity in EB-R2, PPM3-EB, and l-LNv neurons (sampling rate, 1Hz). (**d**) Average Ca^{2+} activity traces from (c) aligned by (left) PPM3-EB peak and (right) l-LNv peak. (**e**) As in (d), average Ca^{2+} activity traces from all flies (n = 8 flies). (**f**) Correlation of Ca^{2+} activity (Pearson's r) between EB and PPM3 is considerably stronger than that between EB and l-LNv (p=0.0009, paired t-test after Fisher's Z-transform). (**g**) Group-averaged actograms of control (left) and flies expressing tetanus toxin (TeTn) in PPM3-EB neurons to block

neurotransmission (right). (**h**) Average rhythm strength (power) of genotypes in (g) for 9 days under DD; asterisk denotes significant differences compared to control ($P < 0.0001$, Mann-Whitney test). (**i-j**) Daily Ca^{2+} activity patterns of circadian neurons (top) and EB-R2 neurons (bottom) under DD1 in (i) WT (n = 6 flies) and (j) flies with TeTn expressed in PPM3-EB neurons (n = 6 flies). (**k**) Average rhythm strength (power) of genotypes for 9 days under DD in which DA receptors are knocked down in EB-RNs using *R56H10-GAL4*; asterisk denotes significant differences compared to control ($P < 0.05$, Kruskal-Wallis test followed by post hoc Dunn's tests). (**l**) Model of the circadian output pathway for locomotor activity rhythms: circadian pacemaker M cells and E cells independently activate EB-RN pre-motor circuits around dawn and dusk through the relay of PPM3-EB dopaminergic neurons.

Extended Data Figure Legends

Extended Data Figure 1. The different subgroups of ellipsoid body (EB) ring neurons do not display circadian pacemaker cell properties. (**a**) Confocal images of different subgroups of EB ring with different concentric arborization radii featured by different genetic drivers: the *cry-LexA* pattern did not overlap with that the *pdfr(F)-GAL4 pattern*; the *cry-LexA* pattern did not overlap with the *pWF22-6* pattern (R4d subgroup, see Renn *et al.,* 1999); the *GMR19C08(pdfr)-lexA* pattern did not overlap with the pattern of *pWF22-6*; the *cry-LexA* pattern did overlap with the that of *GMR69F08-GAL4* (R2 subgroup, see Liu *et al.,* 2016); Scale bars, 20 µm. (**b**) Daily Ca^{2+} activity patterns of the EB-RN subgroup R4, labelled by split-GAL4 drivers which caused the strongest effect on increasing locomotor activity (Robie *et al*., 2017). (**c**) Immunostaining of PER protein in the *cry-LexA, LexAop-GCaMP6s* fly at ZT0. Scale bars, 20 µm. PER can be detected in circadian pacemaker neurons, but not in EB-RNs. (**d-f**) Average

397 locomotor activity of (d) wild type (WT, n = 16 flies), (e) flies with Shaggy (SGG) expressed in
398 s-LNv and three out of six LNd with *pdfr(B)-GAL4* (n = 16 flies), and (f) flies with SGG
399 expressed in EB-R3 neurons with *pdfr(F)-GAL4* (n = 32 flies) under LD cycles and in the first
400 day under DD (DD1). Accelerating molecular clocks in M and E cells (e) advanced both morning
401 and evening behavioral phases, yet SGG over-expression in EB-RN neurons (f) was
402 inconsequential.
403
404 **Extended Data Figure 2. EB-RNs respond to circadian neuron activation.** (**a**) Left, map of
405 EB-RNs and circadian pacemaker neurons. Right, average traces of EB-R3 neurons responding
406 to increase of temperature in flies with dTrpA1 expressed in PDF neurons (red, n = 7 flies) and in
407 control flies without dTrpA1 expression (blue, n = 4 flies). Red aspect indicates duration of
408 temperature increase. (**b**) Responses of EB-RNs labelled by *R56H10-GAL4* to ATP application in
409 flies with P2X2 expressed in PDF neurons (left, n = 5 flies) and in control flies without P2X2
410 expression (right, n = 3 flies). Red aspect indicates duration of ATP application. Above, example
411 image baseline Ca^{2+} signal and maximum Ca^{2+} signal changes. Below, average traces of EB ring
412 neurons. (**c**) Maximum Ca^{2+} signal changes after ATP application in individual EB-RNs in (b).
413 (**d**) Responses of EB-R2 neurons, and circadian pacemaker neurons labelled by *cry-LexA,* to ATP
414 application in flies with P2X2 expressed in s-LNv (left, n = 6 flies). (**e**) Responses of EB-R2
415 neurons and circadian pacemaker neurons labelled by *cry-LexA* to ATP application in flies with
416 P2X2 expressed in E cells: three LNd and the 5^{th} s-LNv neurons (left, n = 5 flies) and (**f**) in
417 control flies without P2X2 expression (right, n = 3 flies).
418

Extended Data Figure 3. Daily activity phases of output circuits are dictated by different groups of circadian neurons. (**a**) Average locomotor activity in DD1 of flies expressing SGG in E pacemaker neurons, entrained under 12hr light: 12hr dark cycles (E-cells>SGG, n = 8 flies). (**b**) Phases comparisons between WT and E-cells>SGG flies. Note that both morning and evening activity phases were advanced (Watson-Williams test). (**c**) Daily Ca^{2+} activity patterns of (left) circadian pacemaker neurons and (right) EB-R2 neurons in E-cells>SGG flies under DD (n = 5 flies). (**d**) Phase comparisons of circadian pacemaker neurons between WT and E-cells>SGG. E cells (LNd) were shifted in E-cells>SGG. (**e**) Both the morning peak and the evening peak of EB-R2 were shifted in E-cells>SGG (*$p < 0.05$, Watson-Williams test).

Extended Data Figure 4. Tests of connections from PDF neurons to PPM3-EB and to EB-RNs. (**a**) Above, map of PPM3-EB DA neurons, EB-RNs, and circadian pacemaker neurons. Below-left, average traces of PDF neurons, PPM3-EB neurons, and EB-R1 neurons responding to activation of P2X2-expressing PDF neurons by ATP at two zeitgeber time points: ZT1 (n = 5 flies) and ZT12 (n = 4 flies). Below-right, response latency (onset time constant) of EB-RNs is longer than that of PPM3-EB neurons (p=0.0029, Mann-Whitney test). (**b**) As in Figure 5b-f, dual-color Ca^{2+} imaging: GCaMP6s in PPM3-EB and jRGECO1a in EB-R2 and circadian pacemaker neurons. Below-left, average traces of PPM3-EB neurons, EB-R2 neurons, and circadian pacemaker neurons responding to the bath-application of neuropeptide PDF (10^{-5} M) at two zeitgeber time points: ZT0 (n = 3 flies) and ZT6 (n = 3 flies). Below-right, maximum Ca^{2+} signal changes in individual cells after PDF bath application. (**c**) Average traces of EB-RNs responding to the bath-application of dopamine (10^{-4} M) at ZT6 (n = 4 flies). (**d**) Average traces of EB-R2 neurons, and circadian pacemaker neurons labelled by *cry-LexA,* responding to

activation of P2X2-expressing PPM3-EB DA neurons by ATP (n = 5 flies). Red aspect indicates duration of drug application. Error bars denote SEM.

Extended Data Figure 5. PER protein rhythms of control flies and flies expressing tetanus toxin (TeTn) in PPM3-EB neurons in Figure 5G. (**a**) Representative images of immunostaining against PDF and PER at two different time points: ZT0 and ZT12 of flies expressing TeTn in PPM3-EB. (**b**) Quantification of PER protein staining intensity at four different time points in five groups of circadian neurons from control flies and flies expressing TeTn in PPM3-EB (n > 3 flies for each time points).

Extended Data Table 1. Manipulation of dopamine signaling impairs circadian locomotor activity rhythms. AR, arrhythmic. Period and power are calculated by $\chi 2$ periodogram. Activity represents averaged activity count per 30 min.

Extended Data Table 1. List of driver/ reporter lines used in this study. The nomenclature of ellipsoid body ring neuron (EB-RN) subgroups used in this study – different from that in Omoto *et al.* (2017) - are here indicated.

Methods

Data reporting. No statistical methods were used to predetermine sample sizes. The selection of flies from vials for imaging and behavioral tests were randomized. The investigators were not blinded to fly genotypes.

Fly stocks. Flies were reared on standard cornmeal/agar food at room temperature. Before imaging experiments, flies were entrained under 12 h light: 12 h dark (LD) cycles at 25°C for at least 3 days or under 10 h light: 14 h dark (short day, SD) cycles at 25°C for at least 5 days. The following fly lines were previously described: *tim(UAS)-GAL4* (Blau & Young 1999), *pdfr(F)-GAL4* and *pdfr(B)-GAL4* (Im & Taghert 2011), *GMR56H10-GAL4* (Sun *et al.,* 2017), *GMR69F08-GAL4* (Liu *et al.,* 2016), *dvpdf-GAL4* (Bahn *et al.,* 2009); split-GAL4 lines: GMR_MB122B and GMR_SS00681 (Liang *et al.,* 2017), GMR_SS002769 (Robie *et al.,* 2017); *cry-LexA* (Liang *et al.,* 2017), *pdf-LexA* (Shang *et al.,* 2008); *TH-Flp* (Xie *et al.,* 2018), *pdf-GAL80* (Stoleru *et al.,* 2004); *UAS-SGG* (Martinek *et al.,* 2001), *UAS-P2X2* and *LexAop-P2X2* (Yao *et al.,* 2002), *LexAop-jGECO1a* (Dana *et al.,* 2016), *UAS-GCaMP6s* and *LexAop-GCaMP6s* (Chen *et al.,* 2013), *UAS-DopR1-miRNA* and *UAS-DopR2-miRNA* (Liu *et al.,* 2017), *UAS-D2R-miRNA* and *UAS-DopEcR-miRNA* (Xie *et al.,* 2018); per^{01} (Konopka & Benzer 1971), $norpA^{P24}$ (Ostroy & Pak 1974) and $pdfr^{han5403}$ (Hyun *et al.,* 2005). *UAS-(FRT.stop)-TeTn* (BL67690), *GMR19C08-LexA* (BL52543), *GMR56H10-GAL4* (BL61644), and *GMR92G05-GAL4* (BL48416) were obtained from Bloomington Stock Center. The *cry-LexA* line was a gift from Dr. F Rouyer (CNRS Gyf, Paris).

Nomenclature. The nomenclature of ellipsoid body (EB) subgroups in this study follows Renn *et al.,* (1999a), which was revised by Omoto *et al.,* (2017) reflecting the introduction of more specific driver lines. The EB subgroup labelled by *cry-lexA* and *GMR69F08-GAL4* (also see Liu

482 *et al.,* 2016) was called R2, they were re-named R5 by Omoto *et al.* (2017). The EB subgroup
483 labelled by *GMR19C08(pdfr)-lexA* was called R4, they were re-named R2 by Omoto *et al.*
484 (2017).

485 ***In vivo* fly preparations.** The surgical procedure for *Drosophila in vivo* calcium imaging
486 followed methods described in Liang *et al.,* (2016, 2017). Following CO_2 anesthetization, flies
487 were mounted by inserting the neck into a narrow cut in an aluminum foil base. Thus, the foil
488 permitted immersion of the head by saline during preparatory surgery and *in vivo* imaging, while
489 the body remained in an air-filled enclosure. To access circadian pacemaker neurons on one side
490 of the head, a single antenna, a portion of the dorso-anterior head capsule, and a small part of one
491 compound eye were removed from the side ipsilateral to imaging. To access EB-RNs, both
492 antennae and a portion of the dorso-anterior head capsule were removed, while the compound
493 eyes remained intact. The entire surgery was typically ~15 min in duration. For experiments that
494 entailed transection of connectives, or removal of the entire body, the surgery was conducted
495 with fine forceps prior to brain-exposing surgery. The wounds were then closed by application of
496 a bio-compatible silicone adhesive (Kwik-Sil, WPI, USA).

497 ***In vivo* calcium imaging.** Imaging was conducted with custom Objective Coupled Planar
498 Illumination (OCPI) microscopes (Holekamp *et al.,* 2008), as described in Liang *et al.,* (2016,
499 2017). Briefly, OCPI uses a cylindrical lens to generate a ~5µm thick light sheet, which was
500 coupled to the focal plane of the objective. For 24-hr imaging, the objective coupled light sheet
501 was scanned across the fly brain through the cranial window every 10 min to capture stacks of
502 images. Each stack contained 20 to 40 separate images with a step size of 5 to 10 microns. For
503 each image, exposure time was not more than 0.1 s. During 24-hr imaging, fresh hemolymph-
504 like saline (HL3; 5 mM KCl, 1.5 mM CaCl2, 70 mM NaCl, 20 mM MgCl2, 10 mM NaHCO3, 5

mM trehalose, 115 mM sucrose, and 5 mM HEPES; pH 7.1) was perfused continuously (0.1-0.2 mL/min). Light-dark cycle stimulation during *in vivo* calcium imaging was delivered using a white Rebel LED (Luxeon) controlled by an Arduino UNO board (Smart Projects, Italy) as described in Liang *et al.,* (2017). For short term high-frequency imaging, image stacks were captured every 10 s (Extended Data Figure 2a and 4b), every 2 s (Figure 4a, Extended Data Figure 2b-f and 3cd), or every 1 s (Figure 5c-f and Extended Data Figure 3a). For each image, exposure time was not more than 0.04 s. For pharmacological tests, each fly was treated once. After 1 or 5-min baseline recordings, 1mL of 0.1 mM PDF solution, 1 mM dopamine solution, or 10 mM ATP solution (pH adjusted to 7) was manually added to a 9 mL static HL3 bath over a ~2 s period. PDF was purchased from Neo-MPS (San Diego, CA, USA) at a purity of 86%.

Locomotor monitoring during imaging. During 24-hr *in vivo* calcium imaging, *Drosophila* locomotor activity was measured by an infrared detector (LTE-301)/emitter (940nm, LTE-302) circuit. The infrared emitter was aimed toward the body of the fly and the detector received the infrared light transmitted through the fly (shown in Figure 2a). Both the body and leg movements can cause changes in transmitted light intensity. The analog signal from the infrared detector was transmitted through an Arduino UNO board with 100Hz sampling rate. The infrared emitter was shut off for 10 seconds every 10 min, allowing the microscope to acquire complete volume brain scans. The daily fly locomotor activity pattern was then calculated by counting the activity events within each 10-min bin. The activity events were identified by time-points when the infrared detector signal was out of the range for standard deviation by 3-fold. Then the normalized event count trace was aligned with the EB-R2 neuron calcium signal of the same fly (Figure 2c). The Pearson's correlation coefficient between these two signals was calculated. To test their correlation at an hourly time scale, these two signals then were averaged by a method

similar to spike-triggered averaging. 4-hr windows (1 hr before and 3 hr after the trigger point) of calcium signals were aligned by the local maximum (increasing phase) or local minimum (decreasing phase) of calcium signal derivatives. The locomotor signals occurring in these 4-hr windows were then averaged. Analysis was performed using R 3.3.3.

Locomotor activity. To examine the circadian rhythms of locomotor activity, individual flies was monitored using Trikinetics *Drosophila* Activity Monitor (DAM) system for 6 days under light-dark (LD) cycles and then for 9 days under constant darkness (DD) condition. χ^2 periodogram with a 95% confidence cutoff and SNR analysis were used to measure circadian rhythmicity and periodicity (Levine *et al.,* 2002). Arrhythmicity were defined by a power value (χ^2 power at best period) less than 10, width lower than 1, a period less than 18 hrs or more than 30 hrs. To find the phases of morning and evening peaks, each 24-hr day was split into two halves. For LD, it was split at ZT6. For DD1, it was split at the time of the manually selected midday ‘‘siesta’’. Then the morning peak and evening peak were then determined by the maximum activity in each half.

Immunocytochemistry. Immunostaining for PER and β-Gal followed previous descriptions (Liang *et al.,* 2016). Briefly, fly brains were dissected in ice-cold, calcium-free saline and fixed for 15m in 4% paraformaldehyde containing 7% picric acid (v/v) in PBS. Primary antibodies included rabbit anti-PER (1:5000; kindly provided by Dr. M. Rosbash, Brandeis Univ.; Stanewsky *et al.,* 1997) and mouse anti-β-galactosidase (1:1000; Promega, Madison, WI, Cat. #Z3781, Lot #149211). Secondary antisera were Cy3-conjugated (1:1000; Jackson Immunoresearch, West Grove, PA). Images were acquired on the Olympus FV1200 confocal microscope. PER protein immunostaining intensity was measured in ImageJ-based Fiji (Schindelin *et al.,* 2012).

551 **Imaging data analysis.** Calcium imaging data analysis was as described previously (Liang *et al.,*
552 2016, 2017). Images were acquired by a custom software, Imagine (Holekamp *et al.,* 2008) and
553 processed in Julia 0.6 including non-rigid registration, alignment and maximal projection along
554 z-axis. Then ImageJ-based Fiji was used for rigid registration and to manually select regions of
555 interest (ROIs) over individual cells or groups of cells. Average intensities of ROIs were
556 measured through the time course and divided by average of the whole image to subtract
557 background noise. For spontaneous calcium transients, each time trace was then calculated as
558 $dF/F=(F-F_{min})/F_{mean}$. For 24-hr time traces, traces of certain cell type ROIs were first aligned,
559 based on Zeitgeber Time and averaged across different flies. Hartigans' dip test and Silverman's
560 test were used to testify whether the averaged 24-h time traces are unimodal or bimodal
561 (Hartigan & Hartigan, 1985; Silverman, 1981). The phase relationship between traces was
562 estimated by cross-correlation analysis. The 24-hr-clock circular plot of phases reflected both
563 mean peak time and phase relationships of the same cell-group traces from different flies. For
564 neurons with daily bimodal patterns (EB-RNs and PPM3-EB DA neurons), each trace was split
565 into two parts: ZT18-ZT6 (morning) and ZT6-ZT18 (evening) to estimate the morning and
566 evening peak phases respectively. For dual-color imaging traces, all signals were filtered (high-
567 pass, 1/30 Hz). To 'spike'-triggered average simultaneous traces of three cell types (Figure 5de),
568 the peaks of selected cell-type signal were identified by the local maximum of that signal after a
569 low-pass filter (0.2Hz). Unfiltered signals of three cell types were then aligned by these peaks to
570 calculate the averaged traces for individual cell types. For pharmacological calcium responses,
571 each time trace was normalized by the initial intensity (F/F_0). The maximum change was
572 calculated by the maximum difference of normalized intensities between baseline and after drug
573 application. The latency (onset time constant) was calculated by the duration from drug

574 application to the time when the trace reached 63.2% of maximum change. All statistics tests are
575 two-sided. Trace analysis and statistics were performed using R 3.3.3 and Prism 7 (GraphPad,
576 San Diego CA).

577 **References**

578 Andretic R, van Swinderen B, Greenspan RJ. (2005) Dopaminergic modulation of arousal in
579 *Drosophila. Curr Biol. 15*:1165–1175.

580 Bai, L., Lee, Y., Hsu, C.T., Williams, J.A., Cavanaugh, D., Zheng, X., Stein, C., Haynes, P.,
581 Wang, H., Gutmann, D.H., *et al.,*. (2018). A Conserved Circadian Function for the
582 *Neurofibromatosis 1* Gene. *Cell Rep*. *22*, 3416–3426.

583 Birman S. (2005) Arousal mechanisms: speedy flies don't sleep at night. *Curr Biol*. 15:R511–
584 513.

585 Cavanaugh, D.J.J., Geratowski, J.D.D., Wooltorton, J.R.A.R.A., Spaethling, J.M.M., Hector,
586 C.E.E., Zheng, X., Johnson, E.C.C., Eberwine, J.H.H., and Sehgal, A. (2014). Identification of a
587 Circadian Output Circuit for Rest:Activity Rhythms in *Drosophila. Cell 157*: 689–701.

588 Cavey, M., Collins, B., Bertet, C., and Blau, J. (2016). Circadian rhythms in neuronal activity
589 propagate through output circuits. *Nat. Neurosci. 19*: 1–11.

590 Chang HY, Grygoruk A, Brooks ES, Ackerson LC, Maidment NT, Bainton RJ, Krantz DE.
591 (2006) Overexpression of the *Drosophila* vesicular monoamine transporter increases motor
592 activity and courtship but decreases the behavioral response to cocaine. *Mol. Psychiatry*. 11:99–
593 113.

594 Chen, T.-W., Wardill, T.J., Sun, Y., Pulver, S.R., Renninger, S.L., Baohan, A., Schreiter, E.R.,
595 Kerr, R. a, Orger, M.B., Jayaraman, V., *et al.,*. (2013). Ultrasensitive fluorescent proteins for
596 imaging neuronal activity. *Nature 499*: 295–300.

597 Dana, H., Mohar, B., Sun, Y., Narayan, S., Gordus, A., Hasseman, J. P., ... & Patel, R. (2016).
598 Sensitive red protein calcium indicators for imaging neural activity. *Elife*, *5*: e12727.

599 De La Iglesia HO, Meyer J, and Schwartz WJ (2003) Lateralization of circadian pacemaker
600 output: activation of left- and right-sided luteinizing hormone-releasing hormone neurons
601 involves a neural rather than a humoral pathway. *J Neurosci 23*:7412-7414.

602 Donlea, J.M., Pimentel, D., Talbot, C.B., Kempf, A., Omoto, J.J., Hartenstein, V., and
603 Miesenböck, G. (2018). Recurrent Circuitry for Balancing Sleep Need and Sleep. *Neuron*. *97*:
604 378-389

605 Fifel, K., Meijer, J. H., & Deboer, T. (2018). Circadian and Homeostatic Modulation of Multi-
606 Unit Activity in Midbrain Dopaminergic Structures. *Scientific reports 8*: 7765.

607 Froy, O., Gotter, A. L., Casselman, A. L., & Reppert, S. M. (2003). Illuminating the circadian
608 clock in monarch butterfly migration. *Science*, *300*: 1303-1305.

609 Grima, B., Chélot, E., Xia, R., and Rouyer, F. (2004). Morning and evening peaks of activity rely
610 on different clock neurons of the *Drosophila* brain. *Nature 431*: 869–873.

611 Guo, F., Holla, M., Diaz, M. M., & Rosbash, M. (2018). A circadian output circuit controls
612 sleep-wake arousal threshold in *Drosophila*. *bioRxiv*. 298067.

613 Heinze, S., and Reppert, S.M. (2011). Sun Compass Integration of Skylight Cues in Migratory
614 Monarch Butterflies. *Neuron 69*: 345–358.

615 Helfrich-Förster C. (2005) Neurobiology of the fruit fly's circadian clock. *Genes Brain Behav*.
616 *24*: 65-76.

617 Hirsh J, Riemensperger T, Coulom H, Iché M, Coupar J, Birman S. (2010) Roles of dopamine in
618 circadian rhythmicity and extreme light sensitivity of circadian entrainment. *Curr Biol. 20*: 209-14.
619 PMID: 20096587

620 Kalsbeek A, Palm IF, La Fleur SE, Scheer FA, Perreau-Lenz S, Ruiter M, Kreier F, Cailotto C,
621 Buijs RM. (2006) SCN outputs and the hypothalamic balance of life. *J Biol Rhythms. 21*: 458-
622 469.

623 Kaneko, M., and Hall, J.C. (2000). Neuroanatomy of cells expressing clock genes in *Drosophila*:
624 transgenic manipulation of the period and timeless genes to mark the perikarya of circadian
625 pacemaker neurons and their projections. *J. Comp. Neurol. 422*: 66–94.

626 Klose, M., Duvall, L.B.B., Li, W., Liang, X., Ren, C., Steinbach, J.H.H., and Taghert, P.H.
627 (2016). Functional PDF Signaling in the *Drosophila* Circadian Neural Circuit Is Gated by Ral A-
628 Dependent Modulation. *Neuron 90*: 1–14.

629 Kong, E.C., Woo, K., Li, H., Lebestky, T., Mayer, N., Sniffen, M.R., Heberlein, U., Bainton,
630 R.J., Hirsh, J., and Wolf, F.W. (2010). A pair of dopamine neurons target the D1-like dopamine
631 receptor dopr in the central complex to promote ethanol-stimulated locomotion in *Drosophila*.
632 PLoS One *5*: e9954.

633 Konopka, R.J., and Benzer, S. (1971). Clock mutants of *Drosophila melanogaster*. *Proc. Natl.*
634 *Acad. Sci. U. S. A. 68*: 2112–2116.

635 Kudo, T., Loh, D. H., Truong, D., Wu, Y., & Colwell, C. S. (2011). Circadian dysfunction in a
636 mouse model of Parkinson's disease. *Experimental neurology*, *232*: 66-75.

637 Kume K, Kume S, Park SK, Hirsh J, Jackson FR. (2005) Dopamine is a regulator of arousal in
638 the fruit fly. *J Neurosci. 25*:7377–7384.

639 Lamaze, A., Kratschmer, P., and Jepson, J.E.. (2018). A sleep-regulatory circuit integrating
640 circadian, homeostatic and environmental information in *Drosophila. BioRxiv.* 250829.

641 Landgraf D, Joiner WJ McCarthy MJ, Kiessling S, Barandas R, Young JW, Cermakian N, Welsh
642 DK. (2016) The mood stabilizer valproic acid opposes the effects of dopamine on circadian
643 rhythms. *Neuropharmacology*. *107*: 262-270.

644 Lebestky T, Chang JS, Dankert H, Zelnik L, Kim YC, Han KA, Wolf FW, Perona P, Anderson
645 DJ. (2009) Two different forms of arousal in *Drosophila* are oppositely regulated by the
646 dopamine D1 receptor ortholog DopR via distinct neural circuits. *Neuron*. *64*: 522-536.

647 Lehman MN, Silver R, Gladstone WR, Kahn RM, Gibson M, and Bittman EL (1987) Circadian
648 rhythmicity restored by neural transplant. Immunocytochemical characterization of the graft and
649 its integration with the host brain. *J Neurosci 7*: 1626-1638.

650 Liang, X., Holy, T.E., and Taghert, P.H. (2016). Synchronous *Drosophila* circadian pacemakers
651 display nonsynchronous Ca2+ rhythms in vivo. *Science 351*: 976-981.

652 Liang, X., Holy, T.E., and Taghert, P.H. (2017). A Series of Suppressive Signals within the
653 *Drosophila* Circadian Neural Circuit Generates Sequential Daily Outputs. *Neuron 94*: 1173-
654 1189.

655 Lima SQ, Miesenbock G. (2005) Remote control of behavior through genetically targeted
656 photostimulation of neurons. *Cell. 121*: 141–152.

657 Liu Q, Liu S, Kodama L, Driscoll MR, Wu MN. (2012) Two dopaminergic neurons signal to the
658 dorsal fan-shaped body to promote wakefulness in *Drosophila. Curr Biol*. *22*: 2114-2123.

659 Liu, S., Liu, Q., Tabuchi, M., and Wu, M.N. (2016). Sleep Drive Is Encoded by Neural Plastic
660 Changes in a Dedicated Circuit. *Cell* 165: 1347-1360.

661 Luo, A. H., & Aston-Jones, G. (2009). Circuit projection from suprachiasmatic nucleus to ventral
662 tegmental area: a novel circadian output pathway. *European Journal of Neuroscience*, *29*: 748-
663 760.

664 Martín-Peña, A., Acebes, A., Rodríguez, J.R., Chevalier, V., Casas-Tinto, S., Triphan, T.,
665 Strauss, R., and Ferrús, A. (2014). Cell types and coincident synapses in the ellipsoid body of
666 *Drosophila*. *Eur. J. Neurosci*. *39*: 1586–1601.

667 Moore RY, Klein DC. (1974) Visual pathways and the central neural control of a circadian
668 rhythm in pineal serotonin N-acetyltransferase activity. *Brain Res*. 71:17-33.

669 Neuser, K., Triphan, T., Mronz, M., Poeck, B., & Strauss, R. (2008). Analysis of a spatial
670 orientation memory in *Drosophila*. *Nature* *453*: 1244.

671 Nitabach, M.N., and Taghert, P.H. (2008). Organization of the *Drosophila* circadian control
672 circuit. *Curr. Biol*. *18*, R84-93.

673 Ofstad, T. A., Zuker, C. S., and Reiser, M. B. (2011). Visual place learning in *Drosophila*
674 melanogaster. *Nature*, *474*, 204.

675 Omoto, J.J., Keleş, M.F., Nguyen, B.C.M., Bolanos, C., Lovick, J.K., Frye, M.A., and
676 Hartenstein, V. (2017). Visual Input to the *Drosophila* Central Complex by Developmentally and
677 Functionally Distinct Neuronal Populations. *Curr. Biol. 27*, 1098–1110.

678 Pfeiffer, K., and Homberg, U. (2014). Organization and Functional Roles of the Central
679 Complex in the Insect Brain. *Annu. Rev. Entomol. 59*: 2014.

680 Pírez, N., Christmann, B.L., and Griffith, L.C. (2013). Daily rhythms in locomotor circuits in
681 *Drosophila* involve PDF. *J. Neurophysiol. 110*, 700–708.

682 Potdar, S., & Sheeba, V. (2018). Wakefulness Is Promoted during Day Time by PDFR Signalling
683 to Dopaminergic Neurons in *Drosophila melanogaster*. *eNeuro*, 5(4).

684 Ralph MR, Foster RG, Davis FC, and Menaker M (1990) Transplanted suprachiasmatic nucleus
685 determines circadian period. *Science* 247:975-978.

686 Renn, S.C.P., Armstrong, J.D., Yang, M., Wang, Z., An, X., Kaiser, K., and Taghert, P.H.
687 (1999a). Genetic analysis of the *Drosophila* ellipsoid body neuropil: Organization and
688 development of the central complex. *J. Neurobiol. 41*, 189–207.

689 Renn, S.C., Park, J.H., Rosbash, M., Hall, J.C., and Taghert, P.H. (1999b). A *pdf* neuropeptide
690 gene mutation and ablation of PDF neurons each cause severe abnormalities of behavioral
691 circadian rhythms in *Drosophila. Cell* 99: 791–802.

692 Robie, A.A., Hirokawa, J., Edwards, A.W., Umayam, L.A., Lee, A., Phillips, M.L., Card, G.M.,
693 Korff, W., Rubin, G.M., Simpson, J.H., *et al.,*. (2017). Mapping the Neural Substrates of
694 Behavior. *Cell 170*: 393–406.e28.

695 Seelig, J.D., and Jayaraman, V. (2013). Feature detection and orientation tuning in the
696 *Drosophila* central complex. Nature *503*: 262–266.

697 Selcho, M., Millán, C., Palacios-Muñoz, A., Ruf, F., Ubillo, L., Chen, J., Bergmann, G., Ito, C.,
698 Silva, V., Wegener, C., et al. (2017). Central and peripheral clocks are coupled by a neuropeptide
699 pathway in *Drosophila*. *Nat. Commun*. *8*: 15563.

700 Shang, Y., Donelson, N.C., Vecsey, C.G., Guo, F., Rosbash, M., and Griffith, L.C. (2013). Short
701 neuropeptide F is a sleep-promoting inhibitory modulator. *Neuron 80*: 171–183.

702 Shang, Y., Haynes, P., Pírez, N., Harrington, K.I., Guo, F., Pollack, J., Hong, P., Griffith, L.C.,
703 and Rosbash, M. (2011). Imaging analysis of clock neurons reveals light buffers the wake-
704 promoting effect of dopamine. *Nat. Neurosci*. *14*: 889–895.

705 Shiozaki, H.M., and Kazama, H. (2017). Parallel encoding of recent visual experience and self-
706 motion during navigation in *Drosophila. Nat. Neurosci*. *20*: 1395–1403.

707 Sleipness, E. P., Sorg, B. A., & Jansen, H. T. (2007). Diurnal differences in dopamine transporter
708 and tyrosine hydroxylase levels in rat brain: dependence on the suprachiasmatic nucleus. *Brain*
709 *research*, *1129*: 34-42.

710 Smith, A. D., Olson, R. J., & Justice Jr, J. B. (1992). Quantitative microdialysis of dopamine in
711 the striatum: effect of circadian variation. *Journal of neuroscience methods*, *44*: 33-41.

712 Stoleru, D., Nawathean, P., Fernández, M.D.L.P., Menet, J.S., Ceriani, M.F., and Rosbash, M.
713 (2007). The *Drosophila* circadian network is a seasonal timer. *Cell 129*: 207–219.

714 Stoleru, D., Peng, Y., Agosto, J., and Rosbash, M. (2004). Coupled oscillators control morning
715 and evening locomotor behaviour of *Drosophila*. Nature *431*: 862-868.

716 Stoleru, D., Peng, Y., Nawathean, P., and Rosbash, M. (2005). A resetting signal between
717 Drosophila pacemakers synchronizes morning and evening activity. *Nature 438*, 238–242.

718 Strauss, R., and Heisenberg, M. (1993). A higher control center of locomotor behavior in the
719 *Drosophila* brain. *J. Neurosci. 13*: 1852–1861.

720 Sun, Y., Nern, A., Franconville, R., Dana, H., Schreiter, E.R., Looger, L.L., Svoboda, K., Kim,
721 D.S., Hermundstad, A.M., and Jayaraman, V. (2017). Neural signatures of dynamic stimulus
722 selection in *Drosophila*. *Nat. Neurosci. 20*: 1104-1113

723 Sweeney, S. T., Broadie, K., Keane, J., Niemann, H., & O'Kane, C. J. (1995). Targeted
724 expression of tetanus toxin light chain in *Drosophila* specifically eliminates synaptic
725 transmission and causes behavioral defects. *Neuron*, *14*(2), 341-351.

726 Taylor, T. N., Caudle, W. M., Shepherd, K. R., Noorian, A., Jackson, C. R., Iuvone, P. M., ... &
727 Miller, G. W. (2009). Nonmotor symptoms of Parkinson's disease revealed in an animal model
728 with reduced monoamine storage capacity. *Journal of Neuroscience*, *29*(25), 8103-8113.

729 VanderLeest HT, Houben T, Michel S, Deboer T, Albus H, Vansteensel MJ, Block
730 GD, Meijer JH. (2007). Seasonal encoding by the circadian pacemaker of the SCN. *Current*
731 *Biol. 17*: 468-473.

732 van Swinderen B, Andretic R. (2003). Arousal in *Drosophila*. Behavioural Processes. 64:133–
733 144.

734 Videnovic, A., and Golombek, D. (2017). Circadian dysregulation in Parkinson's disease.
735 Neurobiol. Sleep Circadian Rhythm. *2*: 53–58.

736 Wu MN, Koh K, Yue Z, Joiner WJ, Sehgal A. (2008). A genetic screen for sleep and circadian
737 mutants reveals mechanisms underlying regulation of sleep in *Drosophila*. *Sleep. 31*: 465–472.

738 Yao Z, Shafer OT. (2014). The *Drosophila* circadian clock is a variably coupled network of
739 multiple peptidergic units. *Science. 343*:1516-1520.

740 Yoshii, T., Funada, Y., Ibuki-Ishibashi, T., Matsumoto, A., Tanimura, T., and Tomioka, K.
741 (2004). *Drosophila cryb* mutation reveals two circadian clocks that drive locomotor rhythm and
742 have different responsiveness to light. *J. Insect Physiol*. *50*: 479–488.

743 Yurgel, M. E., Kakad, P., Zandawala, M., Nassel, D. R., Godenschwege, T. A., & Keene, A.
744 (2018). A single pair of leucokinin neurons are modulated by feeding state and regulate sleep-
745 metabolism interactions. *BioRxiv*, 313213.

746 Zandawala M, Yurgel ME , Liao S , Texada MJ , Rewitz KF, Keene AC , and Nässel DR (2018)
747 Orchestration of *Drosophila* post-feeding physiology and behavior by the neuropeptide
748 leucokinin. *bioRxiv,* 355107.

Method References

Bahn, J. H., Lee, G. G., & Park, J. H. (2009). Comparative analysis of Pdf-mediated circadian behaviors between Drosophila melanogaster and Drosophila virilis. *Genetics*.

Blau, J., and Young, M.W. (1999). Cycling vrille expression is required for a functional Drosophila clock. Cell *99*, 661–671.

Hartigan, J. A. and Hartigan, P. M. (1985). The Dip Test of Unimodality, Journal of the American Statistical Association, 86, 738–746.

Holekamp, T.F., Turaga, D., and Holy, T.E. (2008). Fast three-dimensional fluorescence imaging of activity in neural populations by objective-coupled planar illumination microscopy. Neuron *57*, 661–672.

Hyun, S., Lee, Y., Hong, S.-T., Bang, S., Paik, D., Kang, J., Shin, J., Lee, J., Jeon, K., Hwang, S., *et al.,*. (2005). Drosophila GPCR Han is a receptor for the circadian clock neuropeptide PDF. Neuron *48*, 267–278.

Im, S.H., and Taghert, P.H. (2010). PDF Receptor Expression Reveals Direct Interactions between Circadian Oscillators in Drosophila. J. Comp. Neurol. *518*, 1925–1945.

Levine, J., Funes, P., Dowse, H., and Hall, J. (2002). Signal analysis of behavioral and molecular cycles. BMC Neurosci. *25*, 1–25.

Liu, Q., Tabuchi, M., Liu, S., Kodama, L., Horiuchi, W., Daniels, J., Chiu, L., Baldoni, D., and Wu, M.N. (2017). Branch-specific plasticity of a bifunctional dopamine circuit encodes protein hunger. Science (80-.). *356*, 534–539.

769 Martinek, S., Inonog, S., Manoukian, A. S., & Young, M. W. (2001). A role for the segment
770 polarity gene shaggy/GSK-3 in the Drosophila circadian clock. *Cell*, *105*(6), 769-779.

771 Ostroy, S. E., & Pak, W. L. (1974). Protein and electroretinogram changes in the alleles of the
772 norp Ap12 Drosophila phototransduction mutant. *Biochimica et Biophysica Acta (BBA)-*
773 *Bioenergetics*, *368*(2), 259-268.

774 Schindelin, J., Arganda-Carreras, I., Frise, E., Kaynig, V., Longair, M., Pietzsch, T., Preibisch,
775 S., Rueden, C., Saalfeld, S., Schmid, B., *et al.* (2012). Fiji: an open-source platform for
776 biological-image analysis. Nat. Methods *9*, 676–682.

777 Silverman, B. W. (1981). Using kernel density estimates to investigate multimodality, Journal of
778 the Royal Statistical Society. Series B, 43, 97–99.

779 Stanewsky, R., Jamison, C.F., Plautz, J.D., Kay, S. a, and Hall, J.C. (1997). Multiple circadian-
780 regulated elements contribute to cycling period gene expression in Drosophila. EMBO J. *16*,
781 5006–5018.

782 Xie, T., Ho, M.C.W., Liu, Q., Horiuchi, W., Lin, C.-C.C., Task, D., Luan, H., White, B.H.,
783 Potter, C.J., and Wu, M.N. (2018). A Genetic Toolkit for Dissecting Dopamine Circuit Function
784 in Drosophila. Cell Rep. *23*, 652–665.

785 Yao, Z., Macara, A.M., Lelito, K.R., Minosyan, T.Y., and Shafer, O.T. (2012). Analysis of
786 functional neuronal connectivity in the Drosophila brain. J. Neurophysiol. 108, 684–696.

787

788 **Acknowledgments:**

789 We thank Cody Greer for building the OCPI-2 microscope, the Holy and Taghert laboratories for
790 advice, and the Washington University Center for Cellular Imaging (WUCCI) for technical
791 support. Heather Dionne, Gerry Rubin, Aljoscha Nern, and Francois Rouyer kindly shared
792 unpublished fly stocks and information. Orie Shafer, Michael Rosbash, the Bloomington Stock
793 Center, and Janelia Research Center provided fly stocks and reagents. The work was supported
794 by the Washington University McDonnell Center for Cellular and Molecular Neurobiology and
795 by NIH grants R01 NS068409 and R01 DP1 DA035081 (T.E.H.), R01 MH067122 (P.H.T.), R24
796 NS086741 (T.E.H. and P.H.T.), NIH Training Grant T32HL110952 (M.C.W.H.), and
797 R01NS079584 (M.W.).

798 **Author contributions**: X.L., M.W., T.H.E., and P.H.T. conceived the experiments; X.L.
799 performed and analyzed all experiments; M.C.W.H. generated and characterized the dopamine-
800 related transgenic fly lines. X.L., M.C.W.H., M.W., T.H.E., and P.H.T. wrote the manuscript.

801 **Competing interests**: The authors declare no competing interests. T.E.H. has a patent on OCPI
802 microscopy.

803 **Materials & Correspondence.**: Materials, raw image data, and codes are available upon request
804 to P.H.T. (taghertp@pcg.wustl.edu).

805

Figure 1

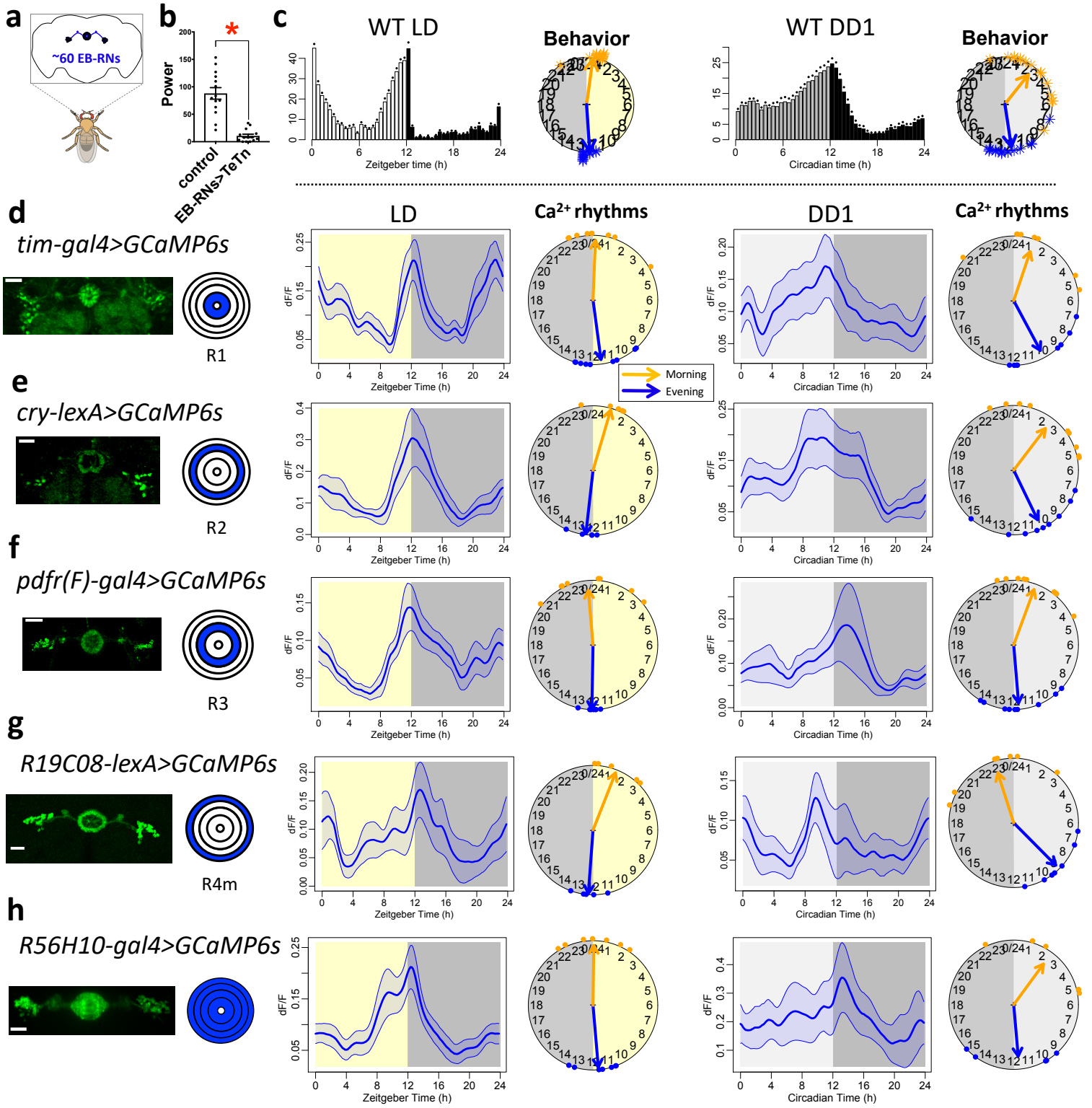

Figure 1. Daily bimodal neural activity patterns of EB ring neurons. (**a**) The ellipsoid body ring neurons (EB-RNs) in the fly brain. (**b**) Average rhythm strength (power) of locomotor activity for 9 days under constant darkness (DD) of control and flies with TeTn expressed in EB-RNs; asterisk denotes significant differences compared to control ($P < 0.0001$, Mann-Whitney test). (**c**) The average locomotor activity histogram and phase distributions of behavioral peaks of wild type *R56H10-gal4/GCaMP6s* flies (left) under 12-hr light: 12-hr dark (LD) cycle and (right) in the first day under DD (n = 16 flies). Dots indicate SEM. (**d**-**h**) Daily Ca^{2+} activity patterns of the EB ring neuron subgroups: (d) R1 labelled by *tim-gal4*, (e) R2 labelled by *cry-lexA*, (f) R3 labelled by *pdfr(F)-gal4*, (g) R4 labelled by *R19H08(pdfr)-lexA*, and (h) R1-4 labelled by *R56H10-gal4*. Left, confocal images of EB ring neurons and diagrams of their concentric arborization radii; scale bars, 25 µm. Middle and Right, average Ca^{2+} transients and Ca^{2+} phase distribution for both morning peaks (orange dots and arrow) and evening peaks (blue dots and arrow). Middle - under LD; Right - under DD.

Figure 2

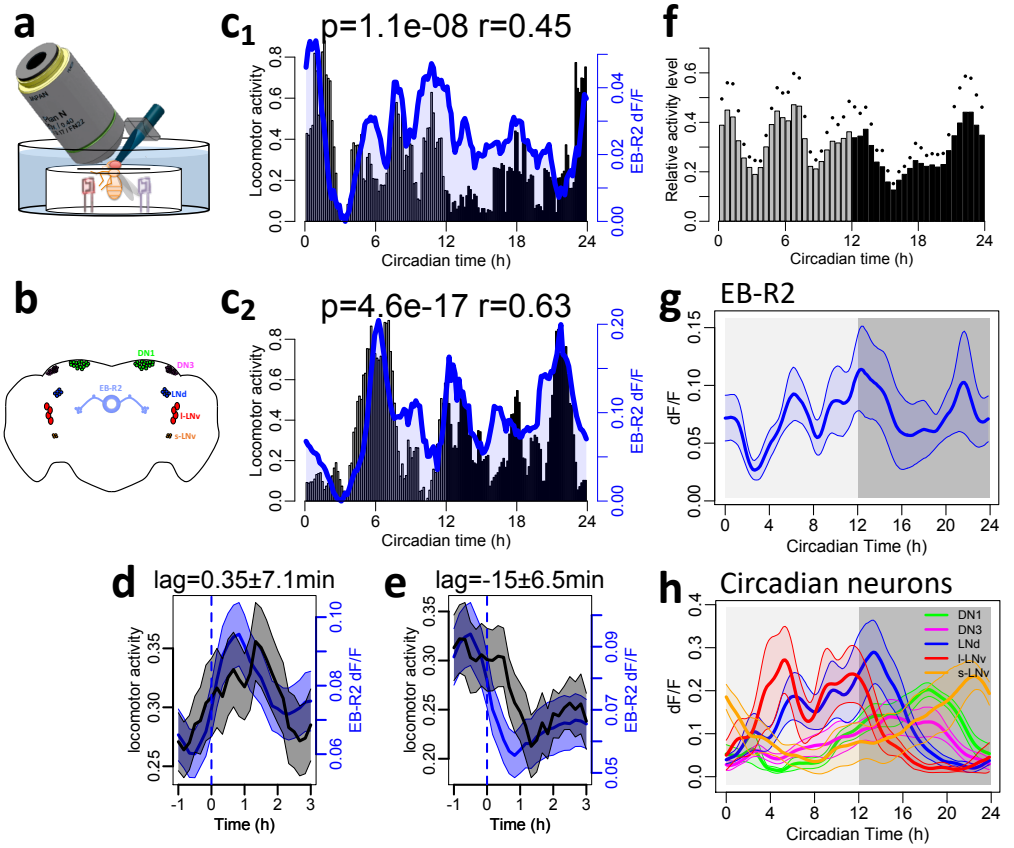

Figure 2. EB ring neuron activity is correlated with locomotor activity. (**a**) Illustration of long-term *in vivo* imaging with infrared measurement of locomotor activity (see Methods). (**b**) Map of the major circadian neuron groups and EB ring neurons. (**c**) Representative recordings of two flies: bars, normalized locomotor activity counts per 10 m; blue traces, Ca^{2+} activity of EB-R2 neurons in the same fly. (**d-e**) Average locomotor activity (black) and Ca^{2+} activity (blue) aligned by (d) increasing phase and (e) decreasing phase of Ca^{2+} activity. The averaged phase lags were calculated by cross-correlation: (c) 0.35±7 min; (d) -15±0.5 min. (**f-h**) Average locomotor activity (f) and average Ca^{2+} transients of (g) EB-R2 neurons and (h) circadian pacemaker neurons in the same flies (n = 6 flies). Dots and shading indicate SEM.

Figure 3

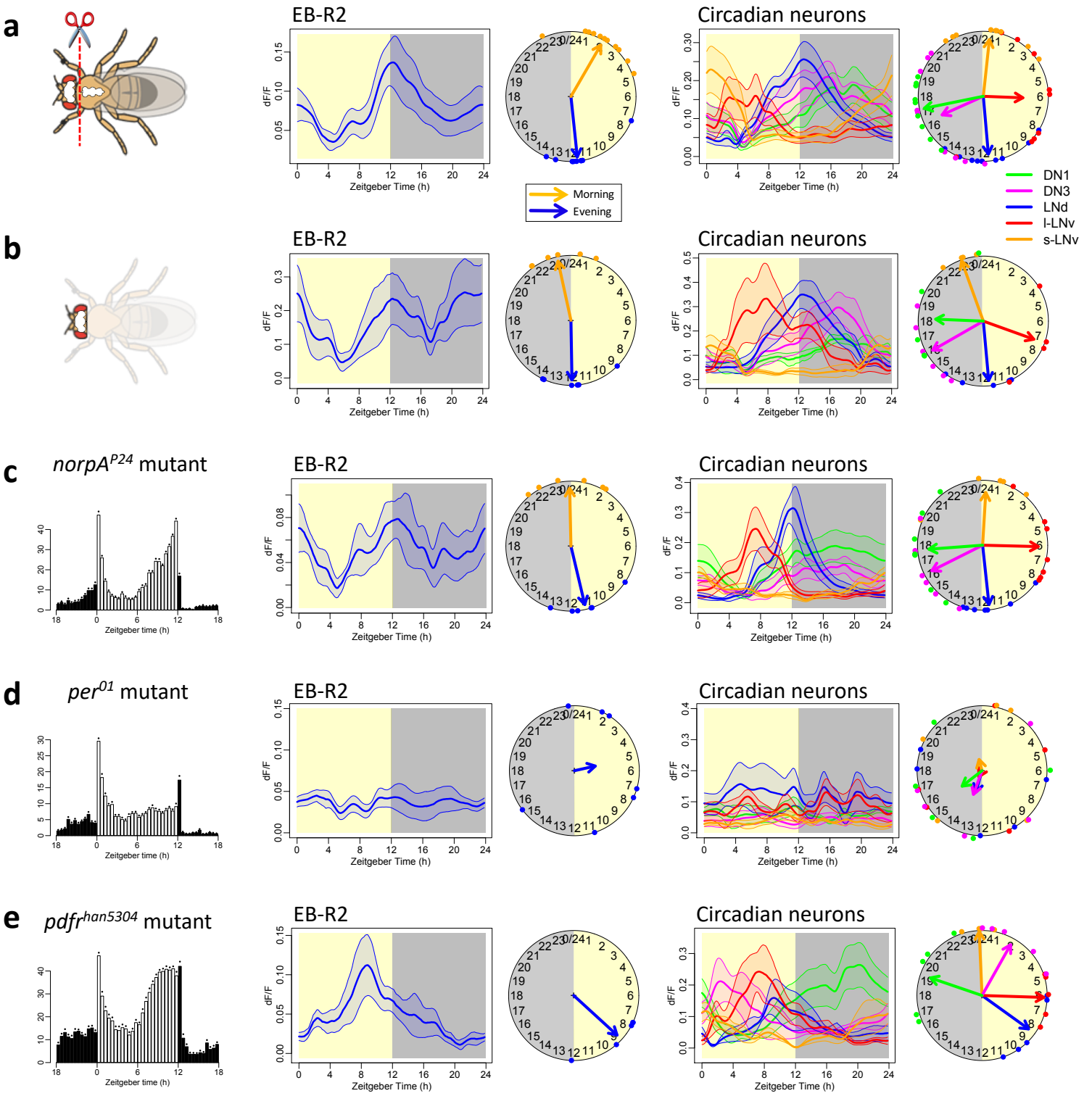

Figure 3. EB ring neuron rhythms are driven by clocks, not in response to behavior. (**a**) Daily Ca^{2+} activity patterns of (middle) EB-R2 neurons and (right) circadian neurons under LD immediately after cutting the connectives between brain and ventral nerve cord (n = 10 flies). (**b**) Daily Ca^{2+} activity patterns of EB-R2 and circadian neurons under LD immediately after removing the bodies (n = 6 flies). (**c**) In blind *norpA*^{P24} mutant flies, (left) average locomotor activity (n = 22 flies) and daily Ca^{2+} activity patterns (middle) of EB-R2 neurons and (right) circadian neurons under LD (n = 6 flies). (**d**) In *per*^{01} mutants, average locomotor activity (n = 16 flies) and arrhythmic Ca^{2+} activity patterns of EB-R2 and of circadian neurons under LD (n = 7 flies). (**e**) In *pdfr*^{han5304} mutants, average locomotor activity (n = 8 flies) and Ca^{2+} activity patterns of EB-R2 and of circadian neurons under LD (n = 7 flies).

Figure 4

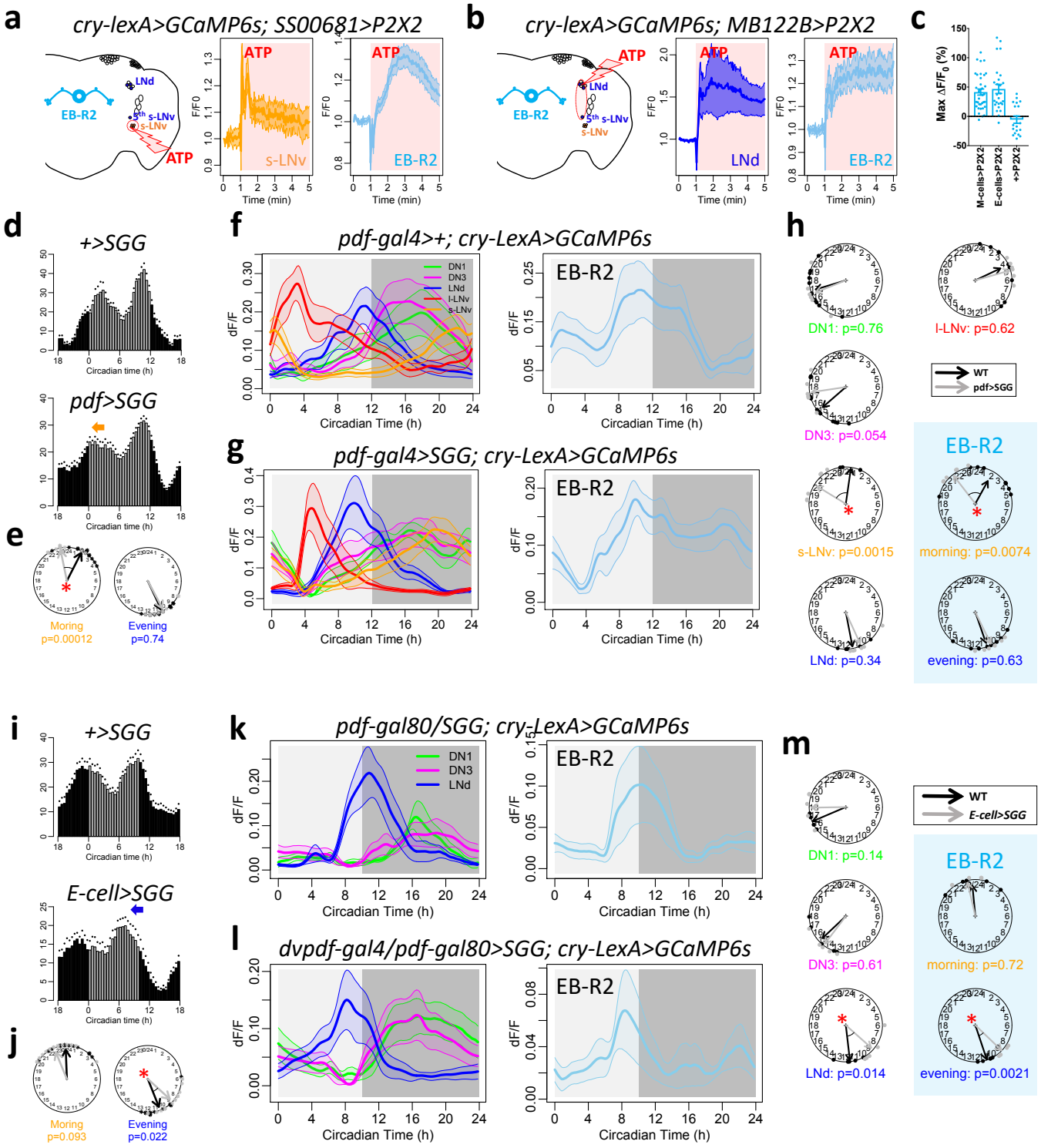

Figure 4. Daily activity phases of EB-RNs are dictated by M and E cells. (**a**) Illustration and averaged response traces of M cells (s-LNv) and EB-R2 neurons to ATP application in flies with P2X2 expressed in M cells (n = 6 flies). (**b**) Illustration and averaged response traces of E cells (three LNd and the 5th s-LNv neurons) and EB-R2 neurons to ATP application in flies with P2X2 expressed in E cells (n = 5 flies). (**c**) Maximum Ca^{2+} changes of EB-R2 after ATP application in (a), (b), and control (n = 3 flies). (**d**) Average locomotor activity in DD1 of (top) wild type (WT, n = 16 flies) and (bottom) flies expressing SGG in PDF neurons (PDF>SGG, n = 24 flies). (**e**) Phases comparisons of morning and evening activity between WT and PDF>SGG. Note that only the morning activity phase was advanced (* $P < 0.05$, Watson-Williams test). (**f-g**) Daily Ca^{2+} activity patterns of (left) circadian neurons and (right) EB-R2 neurons (c) in WT flies under DD (n = 12 flies) and (d) neurons in PDF>SGG flies under DD (n = 6 flies). (**h**) Phase comparison of each circadian neuron group and for both morning peaks (orange) and evening peaks (blue) of EB-R2 neurons between WT and PDF>SGG flies. Note that only M cells (s-LNv) and the morning peak of EB-R2 were significantly advanced in PDF>SGG. (**i**) Average locomotor activity of (top) WT (n = 13 flies) and (bottom) flies expressing SGG in E cells (E-cells>SGG, n = 16 flies) in DD1 after 5 cycles of 10 h light: 14 h dark (short day, SD). **(j)** Phase comparisons of morning and evening activity between WT and E-cell>SGG. Note that only evening activity phases were significantly advanced. (**k-l**) Daily Ca^{2+} activity patterns and phase comparisons of (left) circadian neurons (PDF neurons were invisible due to *pdf-gal80*) and (right) EB-R2 neurons in (k) WT and (l) E-cells>SGG flies after SD entrainment (n = 5 flies). s-LNv and l-LNv were invisible due to *pdf-gal80*. (**m**) E cells (LNd) and the evening peak of EB-R2 were significantly advanced in E-cells>SGG flies compared to WT ones.

Figure 5

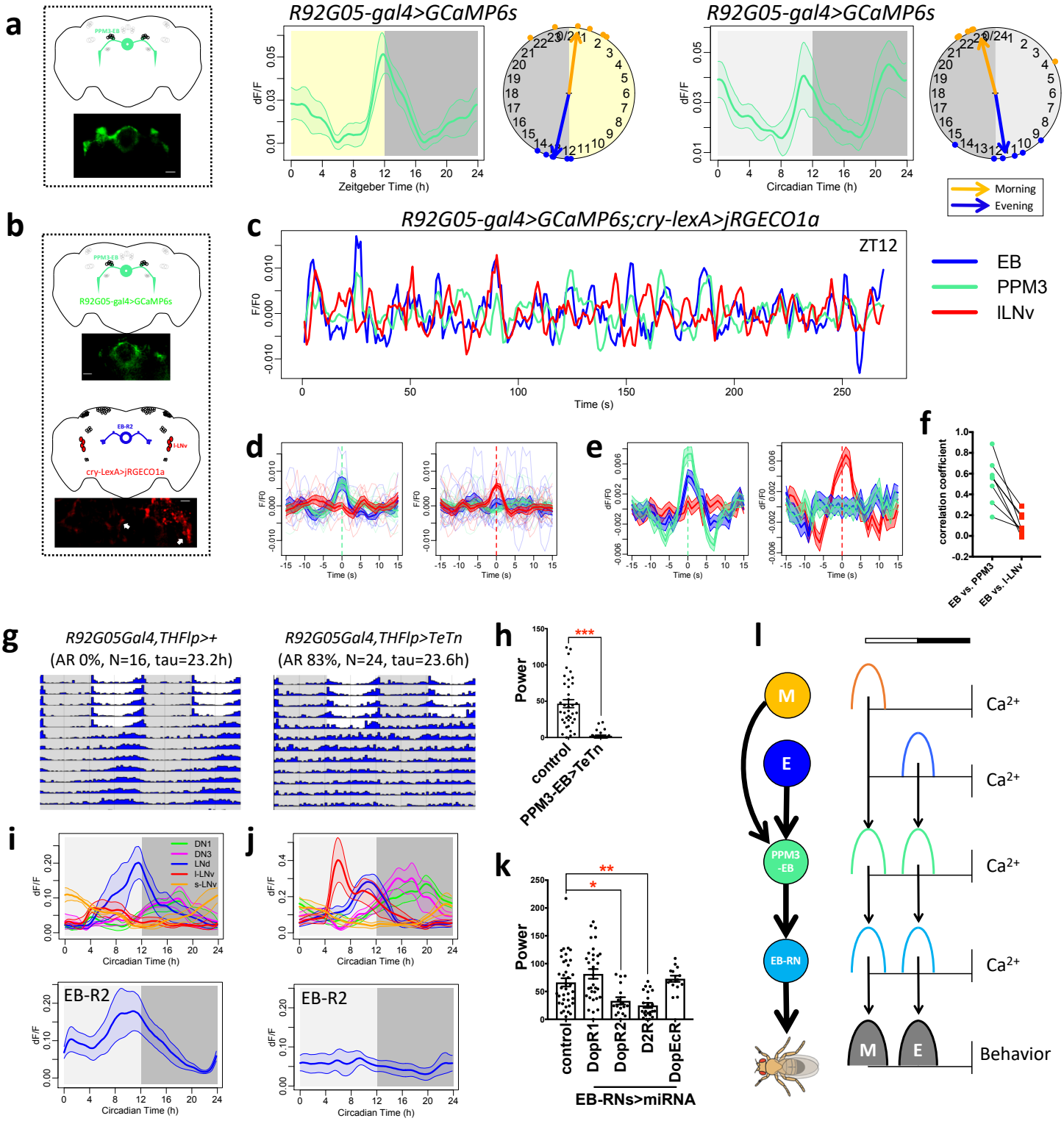

Figure 5. PPM3-EB and EB-RNs constitute a circadian output motor circuit. (**a**) Daily bimodal Ca^{2+} activity patterns of PPM3-EB under LD and DD (n = 6 and 6 flies). (**b**) Illustration of dual-color Ca^{2+} imaging: GCaMP6s in PPM3-EB and jRGECO1a in EB-R2 and circadian neurons. (**c**) Example traces of Ca^{2+} activity in EB-R2, PPM3-EB, and l-LNv neurons (sampling rate, 1Hz). (**d**) Average Ca^{2+} activity traces from (c) aligned by (left) PPM3-EB peak and (right) l-LNv peak. (**e**) As in (d), average Ca^{2+} activity traces from all flies (n = 8 flies). (**f**) Correlation of Ca^{2+} activity (Pearson's r) between EB and PPM3 is considerably stronger than that between EB and l-LNv (p=0.0009, paired t-test after Fisher's Z-transform). (**g**) Group-averaged actograms of control (left) and flies expressing tetanus toxin (TeTn) in PPM3-EB neurons to block neurotransmission (right). (**h**) Average rhythm strength (power) of genotypes in (g) for 9 days under DD; asterisk denotes significant differences compared to control (P < 0.0001, Mann-Whitney test). (**i-j**) Daily Ca^{2+} activity patterns of circadian neurons (top) and EB-R2 neurons (bottom) under DD1 in (i) WT (n = 6 flies) and (j) flies with TeTn expressed in PPM3-EB neurons (n = 6 flies). (**k**) Average rhythm strength (power) of genotypes for 9 days under DD in which DA receptors are knocked down in EB-RNs using *R56H10-gal4*; asterisk denotes significant differences compared to control (P < 0.05, Kruskal-Wallis test followed by post hoc Dunn's tests). (**l**) Model of the circadian output pathway for locomotor activity rhythms: circadian pacemaker M cells and E cells independently activate EB-RN pre-motor circuits around dawn and dusk through the relay of PPM3-EB dopaminergic neurons.

Extended Data Figure 1

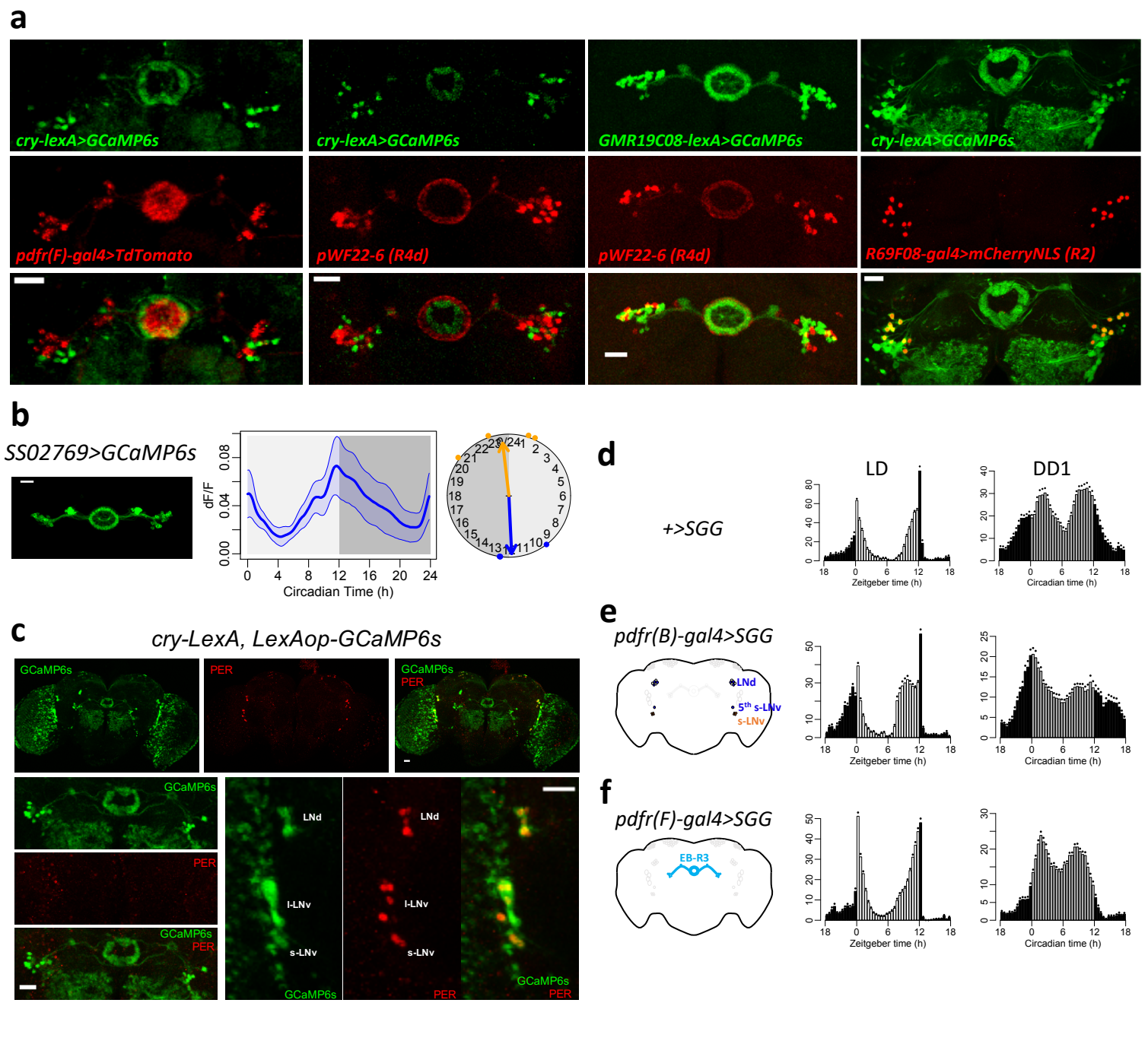

Extended Data Figure 1. The different subgroups of ellipsoid body (EB) ring neurons do not display circadian pacemaker cell properties. (**a**) Confocal images of different subgroups of EB ring with different concentric arborization radii featured by different genetic drivers: the *cry-LexA* pattern did not overlap with that the *pdfr(F)-gal4 pattern*; the *cry-LexA* pattern did not overlap with the *pWF22-6* pattern (R4d subgroup, see Renn et al 1999); the *GMR19C08(pdfr)-LexA* pattern did not overlap with the pattern of *pWF22-6*; the *cry-LexA* pattern did overlap with the that of *GMR69F08-GAL4* (R2 subgroup, see Liu et al 2016); Scale bars, 20 µm. (**b**) Daily Ca^{2+} activity patterns of the EB-RN subgroup R4, labelled by split-gal4 drivers which caused the strongest effect on increasing locomotor activity (Robie *et al*., 2017). (**c**) Immunostaining of PER protein in the *cry-LexA, LexAop-GCaMP6s* fly at ZT0. Scale bars, 20 µm. PER can be detected in circadian pacemaker neurons, but not in EB-RNs. (**d-f**) Average locomotor activity of (d) wild type (WT, n = 16 flies), (e) flies with Shaggy (SGG) expressed in s-LNv and three out of six LNd with *pdfr(B)-GAL4* (n = 16 flies), and (f) flies with SGG expressed in EB-R3 neurons with *pdfr(F)-GAL4* (n = 32 flies) under LD cycles and in the first day under DD (DD1). Accelerating molecular clocks in M and E cells (e) advanced both morning and evening behavioral phases, yet SGG over-expression in EB-RN neurons (f) was inconsequential.

Extended Data Figure 2

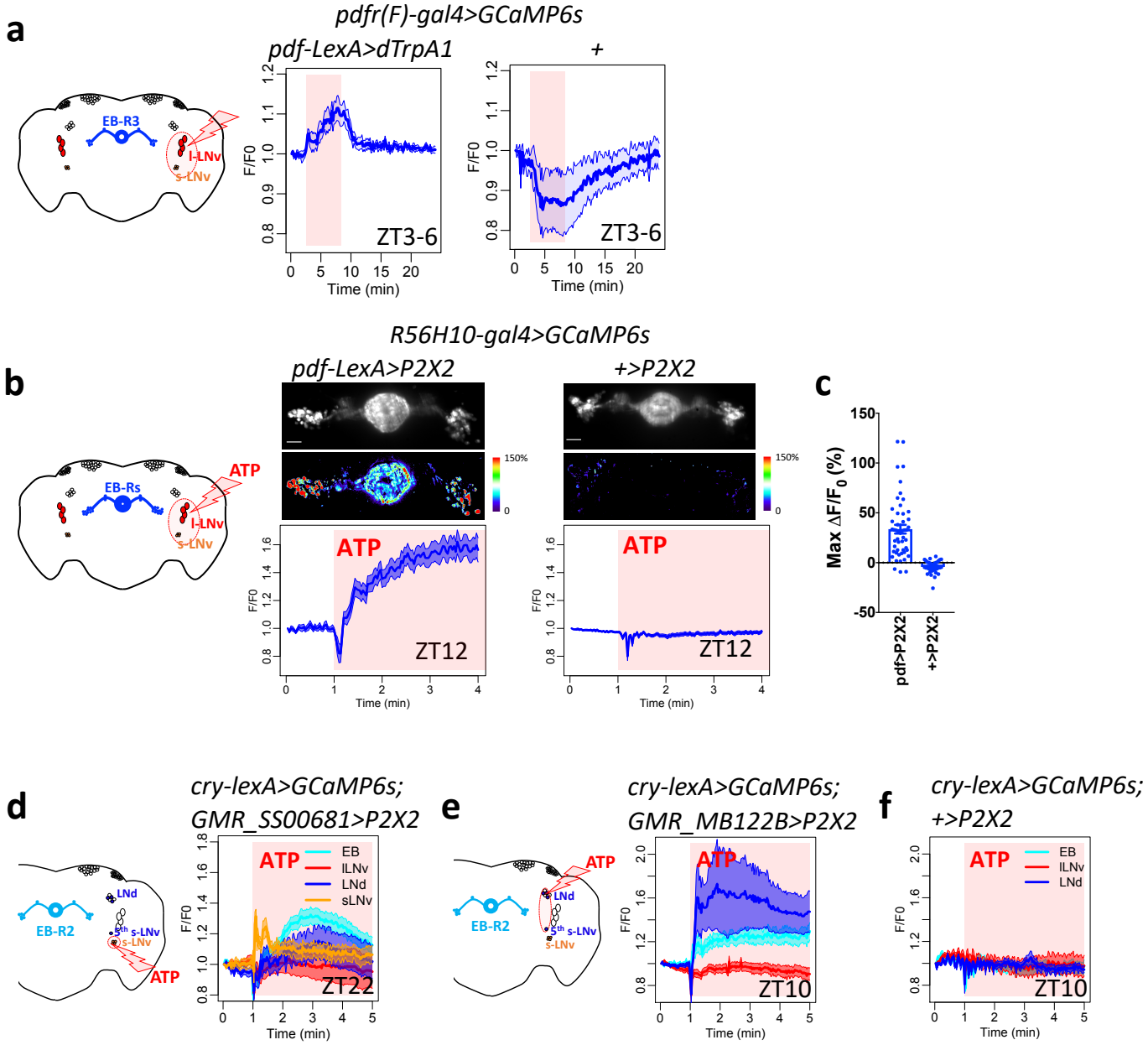

Extended Data Figure 2. EB-RNs respond to circadian neuron activation. (**a**) Left, map of EB-RNs and circadian pacemaker neurons. Right, average traces of EB-R3 neurons responding to increase of temperature in flies with dTrpA1 expressed in PDF neurons (red, n = 7 flies) and in control flies without dTrpA1 expression (blue, n = 4 flies). Red aspect indicates duration of temperature increase. (**b**) Responses of EB-RNs labelled by *R56H10-gal4* to ATP application in flies with P2X2 expressed in PDF neurons (left, n = 5 flies) and in control flies without P2X2 expression (right, n = 3 flies). Red aspect indicates duration of ATP application. Above, example image baseline Ca^{2+} signal and maximum Ca^{2+} signal changes. Below, average traces of EB ring neurons. (**c**) Maximum Ca^{2+} signal changes after ATP application in individual EB-RNs in (b). (**d**) Responses of EB-R2 neurons, and circadian pacemaker neurons labelled by *cry-LexA,* to ATP application in flies with P2X2 expressed in s-LNv (left, n = 6 flies). (**e**) Responses of EB-R2 neurons and circadian pacemaker neurons labelled by *cry-LexA* to ATP application in flies with P2X2 expressed in E cells: three LNd and the 5th s-LNv neurons (left, n = 5 flies) and (**f**) in control flies without P2X2 expression (right, n = 3 flies).

Extended Data Figure 3

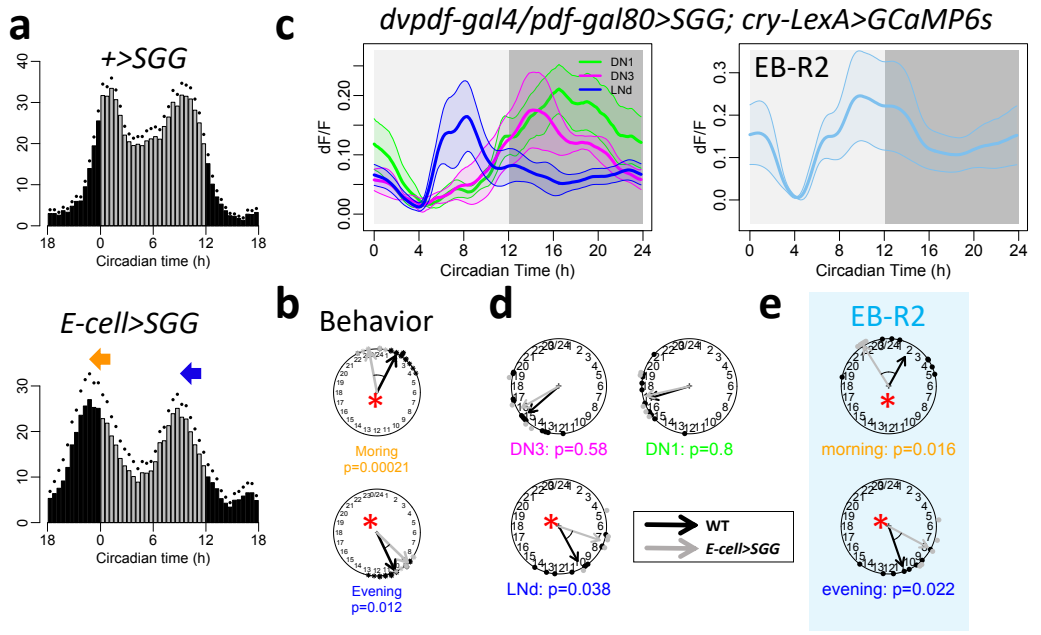

Extended Data Figure 3. Daily activity phases of output circuits are dictated by different groups of circadian neurons. (**a**) Average locomotor activity in DD1 of flies expressing SGG in E pacemaker neurons, entrained under 12hr light: 12hr dark cycles (E-cells>SGG, n = 8 flies). (**b**) Phases comparisons between WT and E-cells>SGG flies. Note that both morning and evening activity phases were advanced (Watson-Williams test). (**c**) Daily Ca^{2+} activity patterns of (left) circadian pacemaker neurons and (right) EB-R2 neurons in E-cells>SGG flies under DD (n = 5 flies). (**d**) Phase comparisons of circadian pacemaker neurons between WT and E-cells>SGG. E cells (LNd) were shifted in E-cells>SGG. (**e**) Both the morning peak and the evening peak of EB-R2 were shifted in E-cells>SGG (*p < 0.05, Watson-Williams test).

Extended Data Figure 4

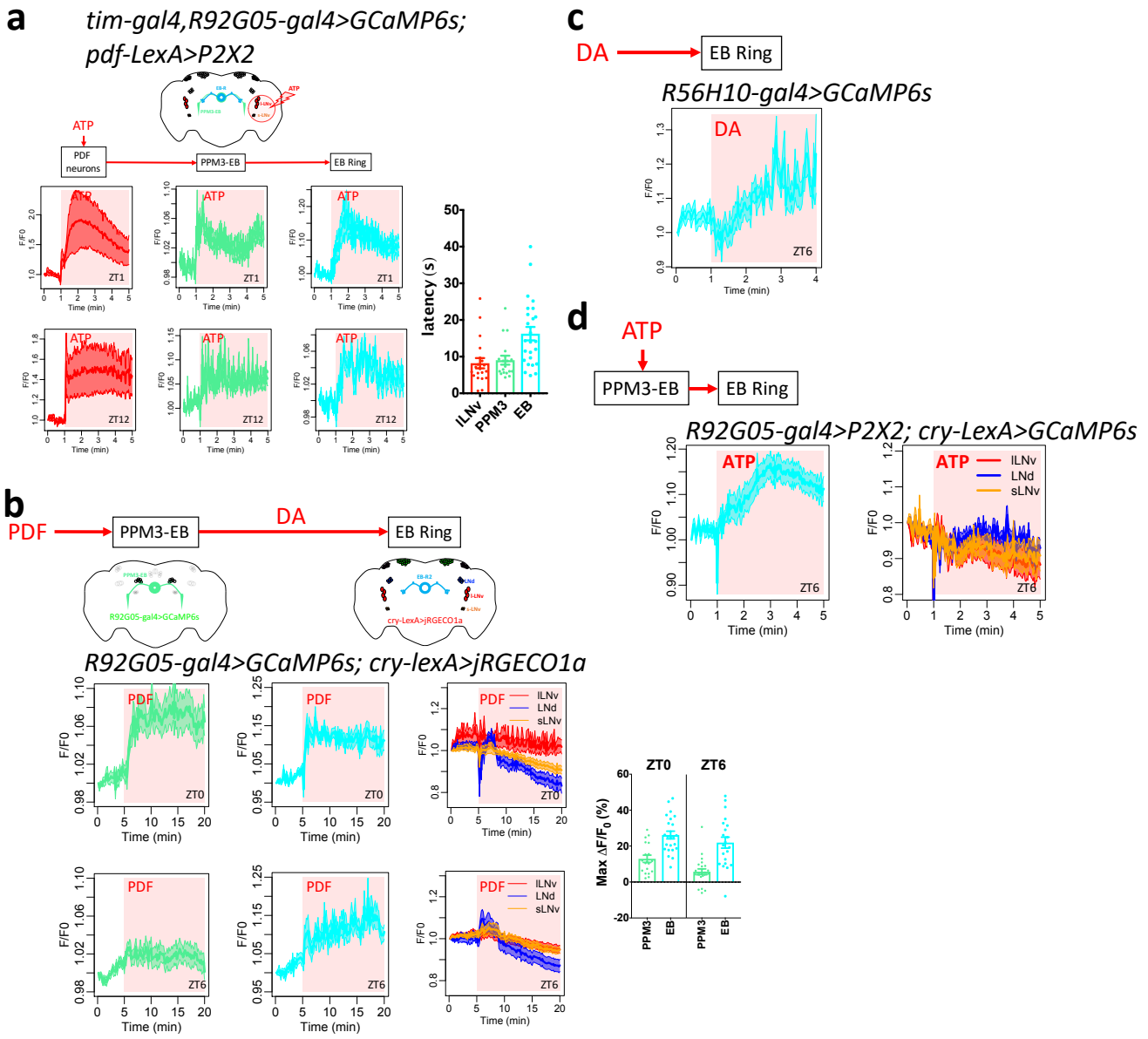

Extended Data Figure 4. Tests of connections from PDF neurons to PPM3-EB and to EB-RNs. (**a**) Above, map of PPM3-EB DA neurons, EB-RNs, and circadian pacemaker neurons. Below-left, average traces of PDF neurons, PPM3-EB neurons, and EB-R1 neurons responding to activation of P2X2-expressing PDF neurons by ATP at two zeitgeber time points: ZT1 (n = 5 flies) and ZT12 (n = 4 flies). Below-right, response latency (onset time constant) of EB-RNs is longer than that of PPM3-EB neurons (p=0.0029, Mann-Whitney test). (**b**) As in Figure 5b-f, dual-color Ca^{2+} imaging: GCaMP6s in PPM3-EB and jRGECO1a in EB-R2 and circadian pacemaker neurons. Below-left, average traces of PPM3-EB neurons, EB-R2 neurons, and circadian pacemaker neurons responding to the bath-application of neuropeptide PDF (10^{-5} M) at two zeitgeber time points: ZT0 (n = 3 flies) and ZT6 (n = 3 flies). Below-right, maximum Ca^{2+} signal changes in individual cells after PDF bath application. (**c**) Average traces of EB-RNs responding to the bath-application of dopamine (10^{-4} M) at ZT6 (n = 4 flies). (**d**) Average traces of EB-R2 neurons, and circadian pacemaker neurons labelled by *cry-LexA,* responding to activation of P2X2-expressing PPM3-EB DA neurons by ATP (n = 5 flies). Red aspect indicates duration of drug application. Error bars denote SEM.

Extended Data Figure 5

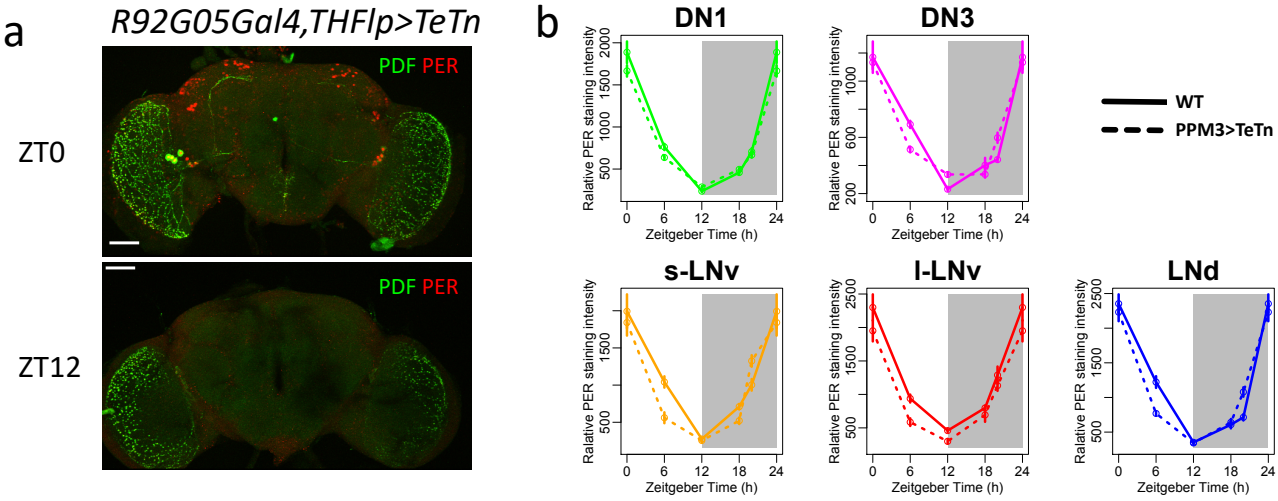

Extended Data Figure 5. PER protein rhythms of control flies and flies expressing tetanus toxin (TeTn) in PPM3-EB neurons in Figure 5G. (**a**) Representative images of immunostaining against PDF and PER at two different time points: ZT0 and ZT12 of flies expressing TeTn in PPM3-EB. (**b**) Quantification of PER protein staining intensity at four different time points in five groups of circadian neurons from control flies and flies expressing TeTn in PPM3-EB (n > 3 flies for each time points).

Extended Data Table 1

Manipulation of dopamine signal and EB-RNs impair circadian locomotor activity rhythms. AR, arrhythmic. Period and power are calculated by χ2 periodogram. Activity represents averaged activity count per 30 min.

Genotype	N	AR	Period (h)	SEM	Power	SEM	Activity	SEM
R56H10-gal4>+	15	7%	23.50	0.10	88.36	10.97	20.53	2.27
R56H10-gal4>UAS-TeTn	14	64%	24.00	0.97	10.69	3.12	6.07	1.25
TH-Flp/+; R92G05-gal4/+	16	0%	23.23	0.12	71.07	7.84	15.69	1.58
TH-Flp/UAS-(FRT.stop)-TeTn;	21	24%	23.17	0.12	22.15	5.01	15.43	1.57
TH-Flp/UAS-(FRT.stop)-TeTn; R92G05-gal4/+	24	83%	23.64	0.05	3.03	1.58	13.85	4.46
R56H10-gal4>+	31	7%	23.31	0.05	67.62	8.35	16.80	1.36
R56H10-gal4>DopR1-miRNA	32	3%	23.63	0.05	84.18	8.57	22.21	1.22
R56H10-gal4>DopR2-miRNA	15	20%	23.56	0.10	33.15	7.17	22.38	1.75
R56H10-gal4>D2R-miRNA	25	12%	23.50	0.10	26.53	4.24	9.41	1.12
R56H10-gal4>DopEcR-miRNA	15	7%	23.57	0.07	72.89	5.54	19.60	1.97

Extended Data Table 2

List of driver/ reporter lines used in this study. The nomenclature of ellipsoid body ring neuron (EB-RN) subgroups used in this study – different from that in Omoto et al. (2017) - are here indicated

Driver / Reporter Lines	EB-RN subgroup	EB-RN subgroup nomenclature by Omoto et al. (2017)	other cell types
tim(UAS)-GAL4	R1	R1	All circadian pacemaker neurons and others
pdfr(F)-GAL4	R3	R3	N/A
cry-LexA	R2	R5	CRY-positive circadian pacemaker neurons and others
GMR69F08-GAL4	R2	R5	N/A*
GMR_SS002769	R2/R4m	R2	N/A
GMR19C08-LexA	R4m	R2	N/A
GMR56H10-GAL4	R1-4	R1-5	N/A
pWF22-6-lacZ	R4d	R4	N/A
pdfr(B)-GAL4	N/A	N/A	all s-LNv, 3 CRY-positive LNd, and 2 DN1
dvpdf-GAL4	N/A	N/A	all LNv and 3 CRY-positive LNd
dvpdf-GAL4, pdf-GAL80	N/A	N/A	the 5th s-LNv and 3 CRY-positive LNd
GMR_SS00681	N/A	N/A	4 PDF-positive s-LNv
GMR_MB122B	N/A	N/A	the 5th s-LNv and 3 CRY-positive LNd
pdf-LexA	N/A	N/A	PDF-positive s-LNv and l-LNv
GMR92G05-GAL4	N/A	N/A	PPM3-EB and others
GMR92G05-GAL4, TH-Flp	N/A	N/A	PPM3-EB

*N/A indicates invisible in the brain